Supporting Information

Orbital overlap-stabilized amorphous metal phosphate frameworks for industrial current density electrocatalysis

Jinyan Xie[a,b], Shiyu Yang[a,b], Ziyong Zhang[a,c], Fei Han[a], Ruizhe Ru[a,b], Lei Zhang[a], Zunming Lu[c], Guowei Li[a], Jun-Qiang Wang*[a,b], Juntao Huo*[a,b]*

J. Xie, S. Yang, Z. Zhang, F. Han, R. Ru, L. Zhang, G. Li, J. Q. Wang, J. Huo

a. Zhejiang Key Laboratory of Magnetic Materials and Applications, Ningbo Institute of Materials Technology and Engineering, Chinese Academy of Science, Ningbo, Zhejiang 315201, China

b. Center of Materials Science and Optoelectronics Engineering, University of Chinese Academy of Sciences, Beijing, 100049, China

Z. Zhang, Z. Lu

c. School of Materials Science and Engineering, Hebei University of Technology, Tianjin 300130, China

E-mail: liguowei@nimte.ac.cn (Guowei Li) or jqwang@nimte.ac.cn (Jun-Qiang Wang) or huojuntao@nimte.ac.cn (Juntao Huo).

Experimental Section

Sample Preparation

The $Fe_{60-x}Co_{10}Ni_{10}P_{20}Ru_x$ (x = 0, 1, 2, 3) alloy ingots were prepared from raw materials of (i) Fe–P alloy and Ru (>99.9 wt.%, Beijing Zhongjin Yan New Materials Technology Co., Ltd.) and (ii) pure Fe, Co and Ni (>99.9 wt.%, Zhongnuo Xincai (Beijing) New Materials Technology Co., Ltd.) by melting the charge in an induction furnace under a high-purity argon atmosphere. Subsequently, amorphous alloy in thin strips with a thickness of about 25 μm and a width of about 1 mm were prepared using melt spinning technology with a copper roller whose spinning tangent speed is about 45 m s^{-1}. The amorphous $Fe_{60-x}Co_{10}Ni_{10}P_{20}Ru_x$ (x = 0, 1, 2, 3) strips is denoted as Rux (x = 0, 1, 2, 3). Electrochemical acid treatment was carried out in 2 M H_2SO_4, and then washed repeatedly with deionized water and anhydrous ethanol to remove residual chemical substances. The dealloyed sample was denoted as Rux-De (x = 0, 1, 2, 3).

Preparation of 20 wt.% Pt/C/NF and RuO_2/NF: 5 mg commercial 20 wt.% Pt/C and RuO_2 nanoparticles were added into a mixed solution of 50 μL Nafion and 950 μL ethanol for ultrasonic dispersion for 30 min to prepare ink. At the same time, 1 cm × 1 cm NF was ultrasonically cleaned in 1 M HCl for 15 min, and then washed three times with deionized water and ethanol respectively. After NF dried, 200 μL ink was dropped onto NF. Finally, dry the NF loaded with catalyst at room temperature.

Characterization

The XRD patterns of quenched and dealloyed thin strips were recorded using D8 ADVANCE under Cu-Kα radiation (λ = 1.5418 A). The TEM analysis was performed on the prepared samples on Talos F200x and Spectra 300. Chemical states were analyzed by XPS using Al-Kα X-ray as the excitation source on Axis Ultra DLD. Perform SEM analysis at 8kV and EDS spectroscopic analysis and elemental mapping at 20 kV on S4800. Perform ICP-OES analysis on Apectro Arcos.

Electrochemical Measurements

The electrochemical performance was studied using a Zennium electrochemical workstation with a three electrode system in 2 M H_2SO_4 solution and 1 M KOH solution, with graphite rods as the counter electrode and Ag/AgCl electrode as the reference electrode. For the convenience of subsequent calculations, the submerged area of the strip is kept at 0.1 cm^2. The current density is standardized by the geometric surface area of the sample. According to the Nernst equation:

$$E_{RHE} = E_{Ag/AgCl} + 0.0591\,pH + 0.2046\#(1)$$

where E_{RHE} is compared to the potential of the reversible hydrogen electrod and $E_{Ag/AgCl}$ is the electrode potential measured when using Ag/AgC as the reference electrod. A stable CV curve was obtained at a scan rate of 200 mV s^{-1}. LSV was performed at a scan rate of 5 mV s^{-1}, and iR loss should be used for correction during LSV measurement. Measure EIS in the frequency range of 100 kHz to 0.01 Hz. Stability tests were conducted using chronoamperometry at 10 mA cm^{-2} and 500 mA cm^{-2}. In addition, the ECSA was measured by CV at scan rates of 20, 40, 60, 80, 100, 120, 140, 160, 180, and 200 mV s^{-1} in the non Faraday potential region. According to the relationship:

$$ECSA = \frac{C_{dl}}{C_S} \#(2)$$

where C_{dl} is electrochemical double-layer capacitance and C_s is specific capacitance. Due to the flat surface of the MG band, the C_s value was assumed to be 0.04 mF cm^{-2}.[1, 2]

The formula for calculating the flip frequency (TOF):

$$TOF = \frac{j \cdot A \cdot Z^{-1} \cdot F^{-1} \cdot N_A}{v_a \cdot ECSA} \#(3)$$

j represents the current density obtained from the polarization curve, Z represents the number of moles of active material (4 for OER, 2 for HER), F is the Faraday constant (98485.3 C mol^{-1}), NA is Avogadro's number (6.022×10^{23} mol^{-1}), and v_a is the amount of active sites on the surface (for alloy materials, generally 1×10^{15}).

The AEM electrolyzer cell utilized in this study has an external dimension of 10 cm × 10 cm, with an internal flow field area of 1cm × 1 cm. A serpentine flow field was employed, and the operating temperature was 80°C (80 ± 2°C). Both the anode and the cathode will splice the strips into suitable sizes for direct use, with nickel foam serving as both the current collector and gas diffusion layer, without any additional gas diffusion layer. We used the Versogen PiperION A20 anion exchange membrane, which has a thickness of 20 micrometers, and it was pre-treated by soaking in 1 M KOH for 24 hours prior to use. The performance of the AEM electrolyzer in a 30 wt.% KOH electrolyte using an four-channel electrochemical workstation (CS310X). The electrolyte flow rate employed for testing was 100 mL min^{-1}. The polarization curve was measured using LSV technique at a scan rate of 5 mV s^{-1}. The durability test was carried out by the CP technique at a current density of 1000 mA cm^{-2}.

Calculation Setup

The first-principles calculations were performed using the Vienna Ab initio Simulation Package (VASP). The interaction between ions and valence electrons was described by the projector augmented wave (PAW) method, and the exchange–correlation energy was treated within the

generalized gradient approximation (GGA) using the Perdew–Burke–Ernzerhof (PBE) functional. To accurately describe the strongly correlated 3d electrons of transition metals, the DFT+U approach within the Dudarev formalism was applied with U_{eff}(Ni) = 6.2 eV and U_{eff}(Co) = 3.32 eV. A plane-wave cutoff energy of 520 eV was adopted to ensure energy convergence. For bulk models, an 8 × 8 × 4 Gamma-centered k-point mesh was used, while a 6 × 1 × 3 k-point grid was employed for surface slab models. The structures were fully optimized until the residual forces on each atom were less than 0.01 eV $Å^{-1}$ and the total energy convergence threshold was set to 10^{-6} eV. In the slab models, a vacuum layer of at least 15 Å was applied along the *z*-direction to prevent spurious interactions between periodic images. For asymmetric slab models, dipole corrections were included to eliminate artificial electrostatic interactions. Spin polarization was taken into account in all calculations. The PDOS was obtained by projecting the Kohn–Sham wave functions onto the Ni 3d, Co 3d, Ru 4d, and O 2p orbitals. The d-band center was calculated according to:

$$\varepsilon_d = \frac{\int E \times D_d(E)\, dE}{\int D_d(E)\, dE} \#(4)$$

where D_d(E) denotes the density of states of the transition-metal d orbitals. Phonon dispersion calculations were carried out using density functional perturbation theory (DFPT) and post-processed with the PHONOPY package.

The formation energy of the Ru-doped structures was calculated to assess their thermodynamic stability, which can be defined as:

$$E_{form} = E_{doped} - E_{host} - \mu_{Ru} + \mu_M \#(5)$$

where E_{doped} and E_{host} denote the total energies of the doped and pristine systems, respectively, and μ_{Ru} and μ_M represent the chemical potentials of Ru and the substituted metal atom.

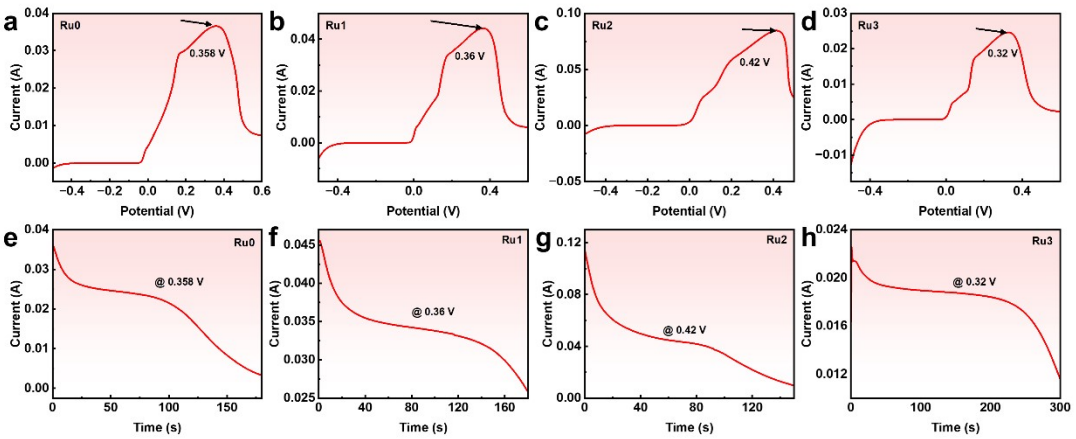

Fig. S1 Electrochemical dealloying parameters of Rux (x=0, 1, 2, 3) amorphous alloy precursor. (a-d) Dealloying voltage. (e-h) Dealloying time.

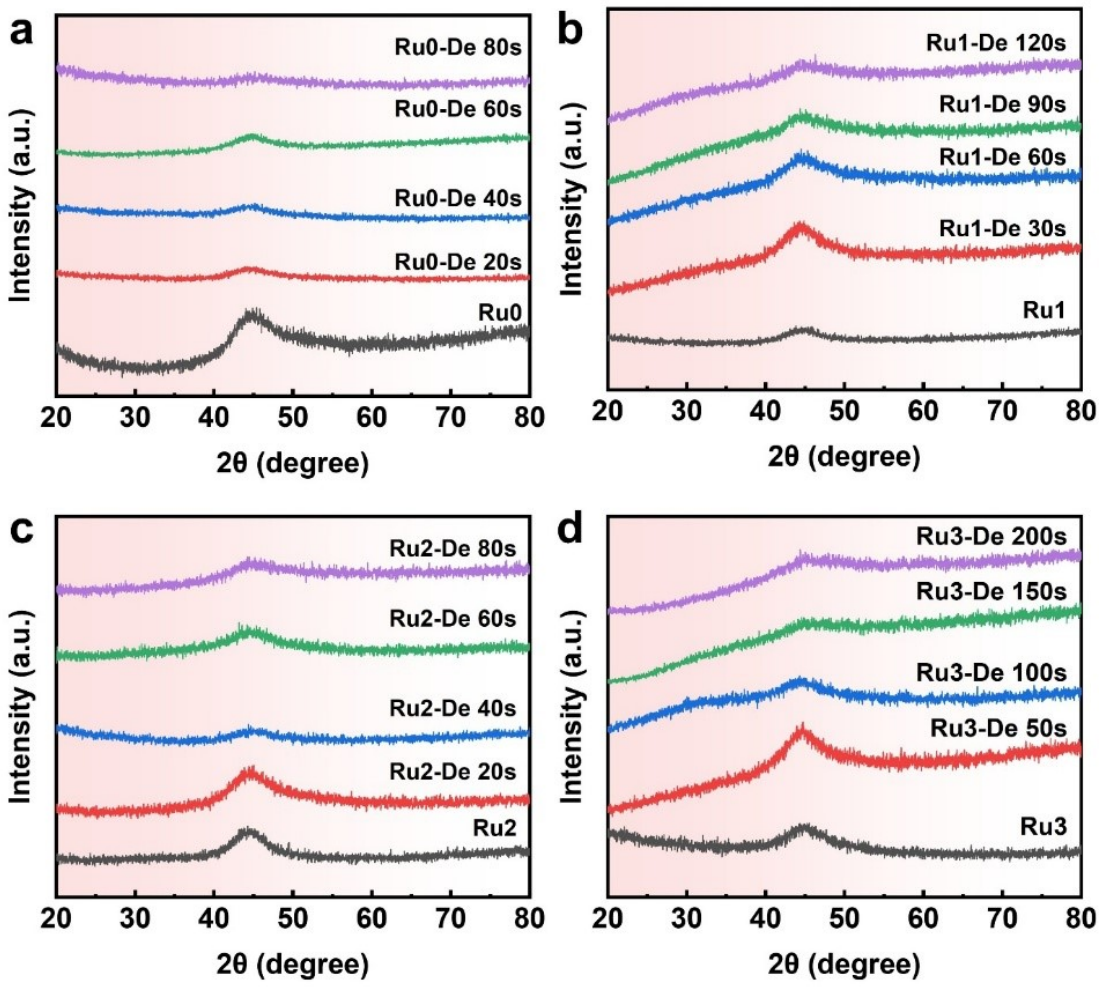

Fig. S2 XRD patterns at different dealloying times. (a) Ru0, (b) Ru1, (c) Ru2, and (d) Ru3.

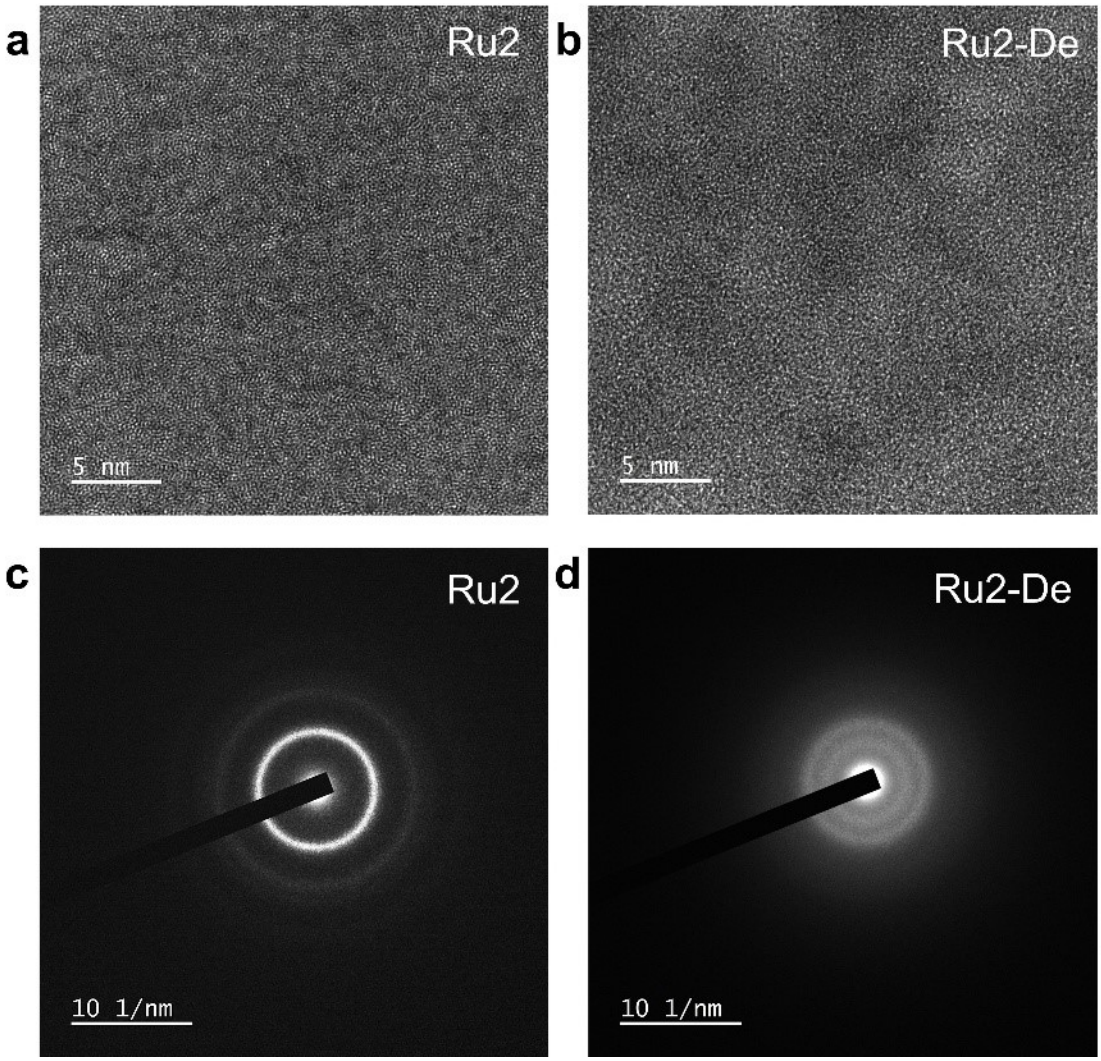

Fig. S3 HRTEM images (a) before and (b) after dealloying treatment. (c) (d) Corresponding SAED patterns.

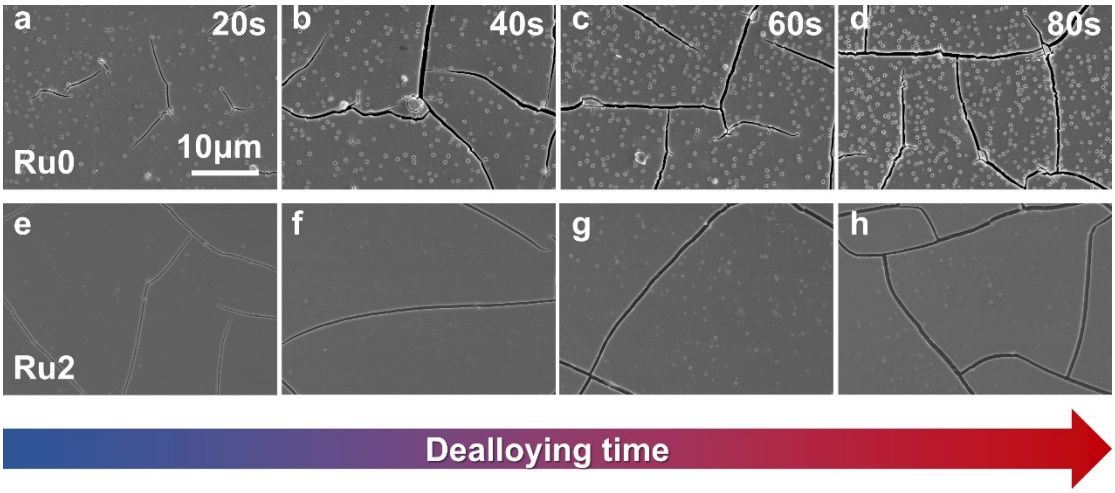

Fig. S4 SEM morphology of surfaces at different dealloying times. (a-d) Ru0, (e-h) Ru2.

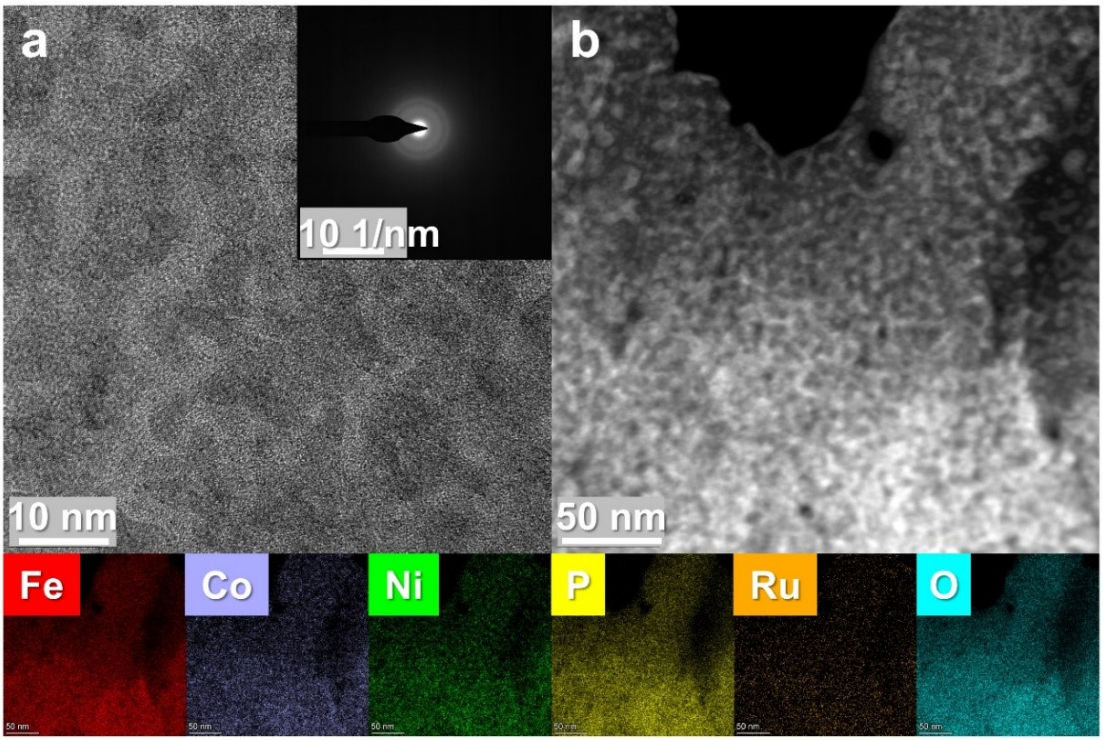

Fig. S5 Structural analysis of Ru2-De. (a) HRTEM image and SAED image. (b) STEM image.

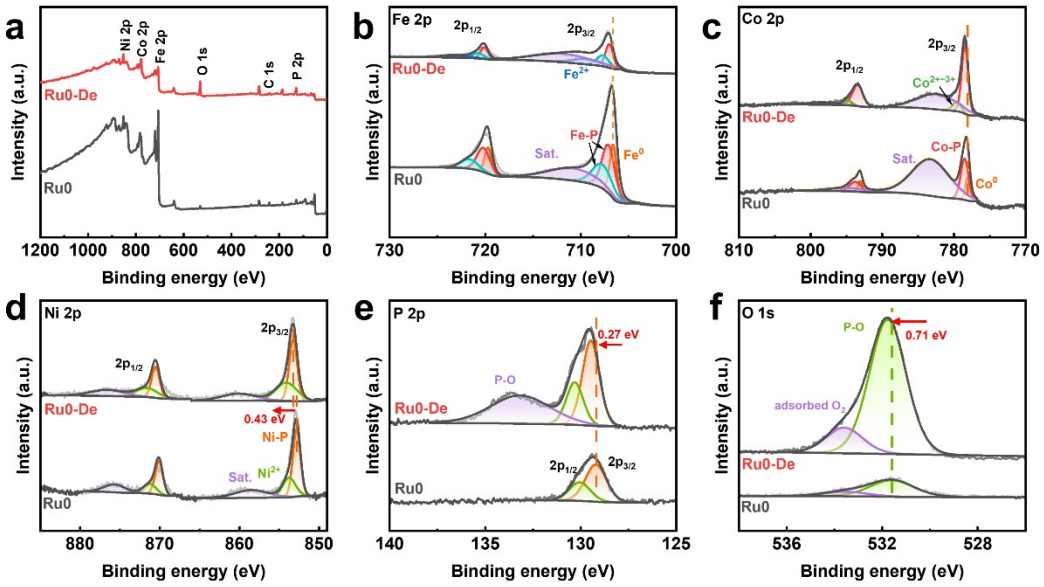

Fig. S6 XPS spectra of Ru0 and Ru0-De. (a) Survey spectrum. high-resolution XPS spectra of (b) Fe 2p, (c) Co 2p, (d) Ni 2p, (e) P 2p and (f) O 2p.

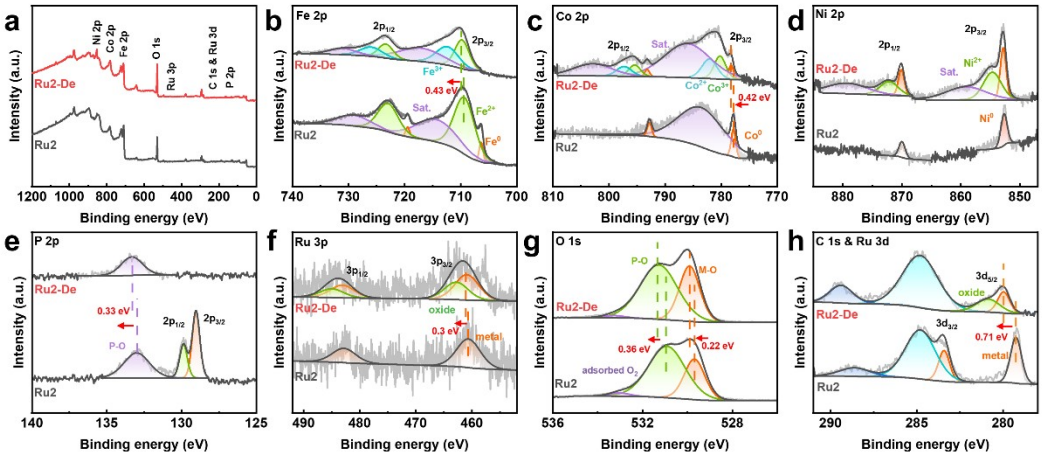

Fig. S7 XPS spectra of Ru2 and Ru2-De. (a) Survey spectrum. high-resolution XPS spectra of (b) Fe 2p, (c) Co 2p, (d) Ni 2p, (e) P 2p, (f) Ru 3p, (g) Ru 3p, (g) O 1s and (h) C 1s & Ru 3d.

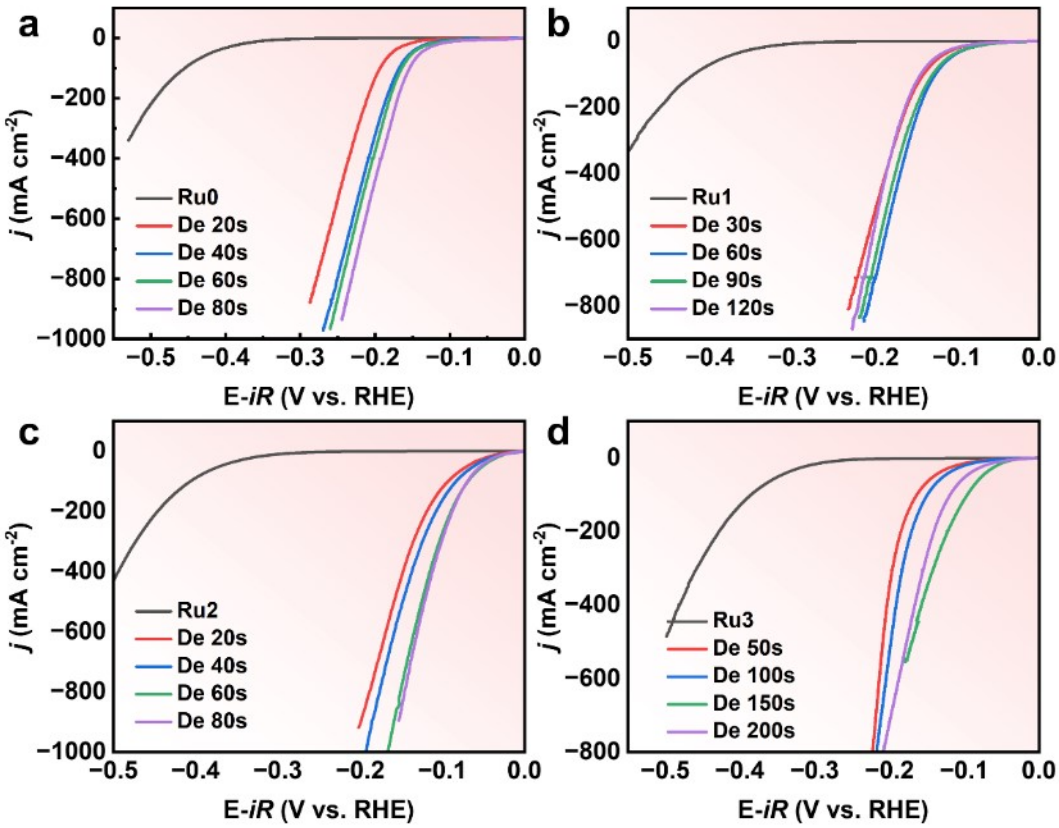

Fig. S8 HER polarization curves of dealloyed samples. (a) Ru0, (b) Ru1, (c) Ru2 and (d) Ru3.

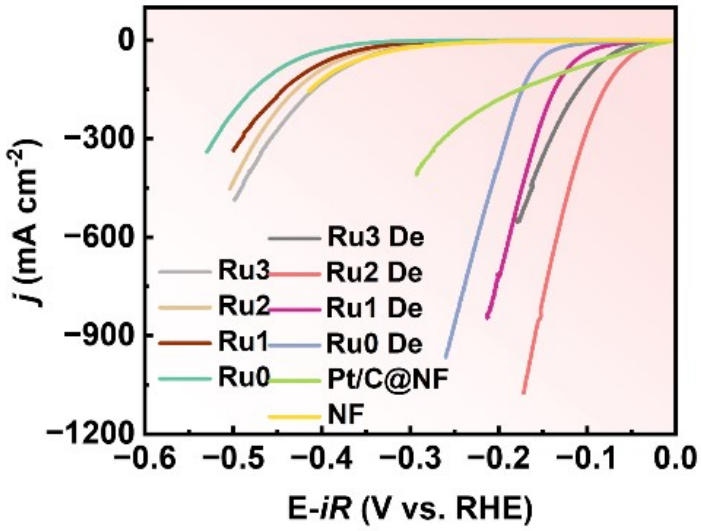

Fig. S9 HER polarization curves of Rux, Rux-De (x=0,1,2,3), Pt/C@NF, and NF.

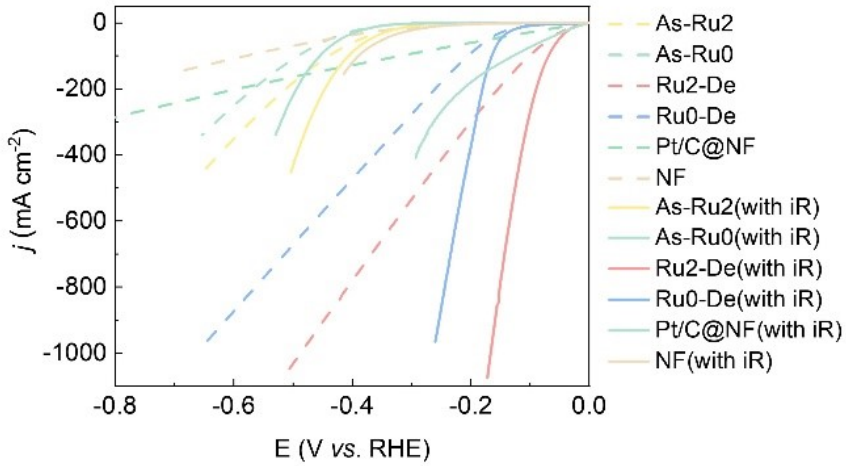

Fig. S10 HER polarization curves of different catalysts (including before and after iR compensation, 95% iR compensation).

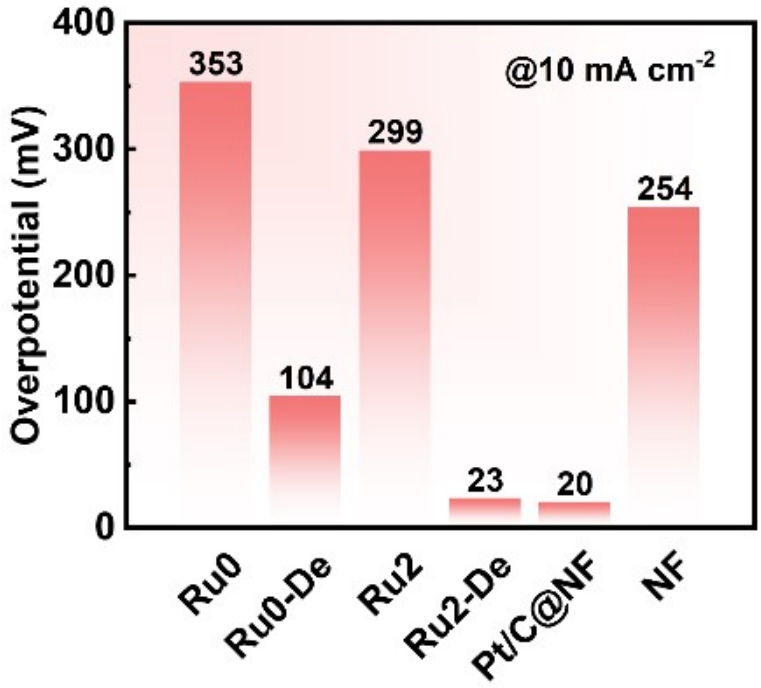

Fig. S11 Comparison of HER overpotentials at 10 mA cm^{-2} for Ru0, Ru0-De, Ru2, Ru2-De, Pt/C@NF, and NF.

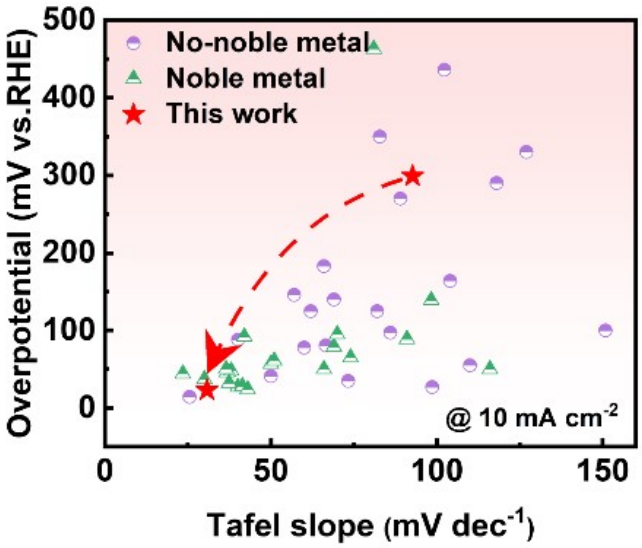

Fig. S12 Comparison of HER activity with recently reported electrocatalysts.

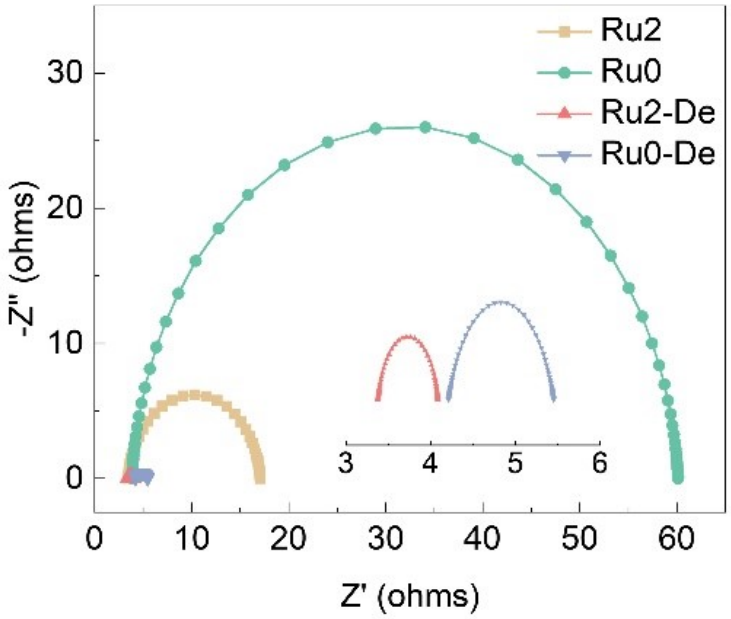

Fig. S13 EIS Nyquist plots for HER.

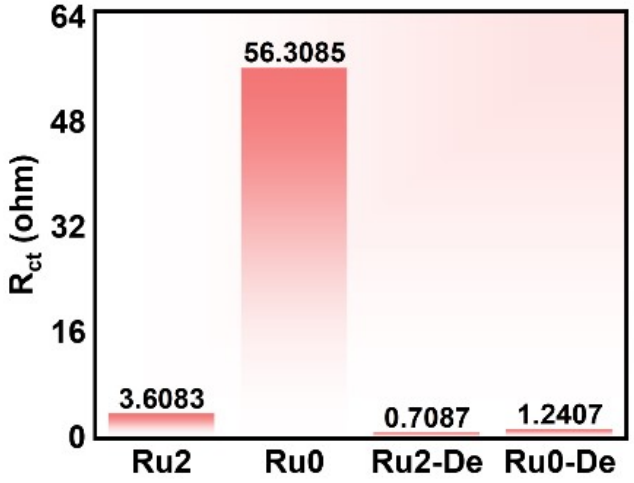

Fig. S14 Comparison of the HER electrochemical transfer resistance of Ru0, Ru0-De, Ru2 and Ru2-De.

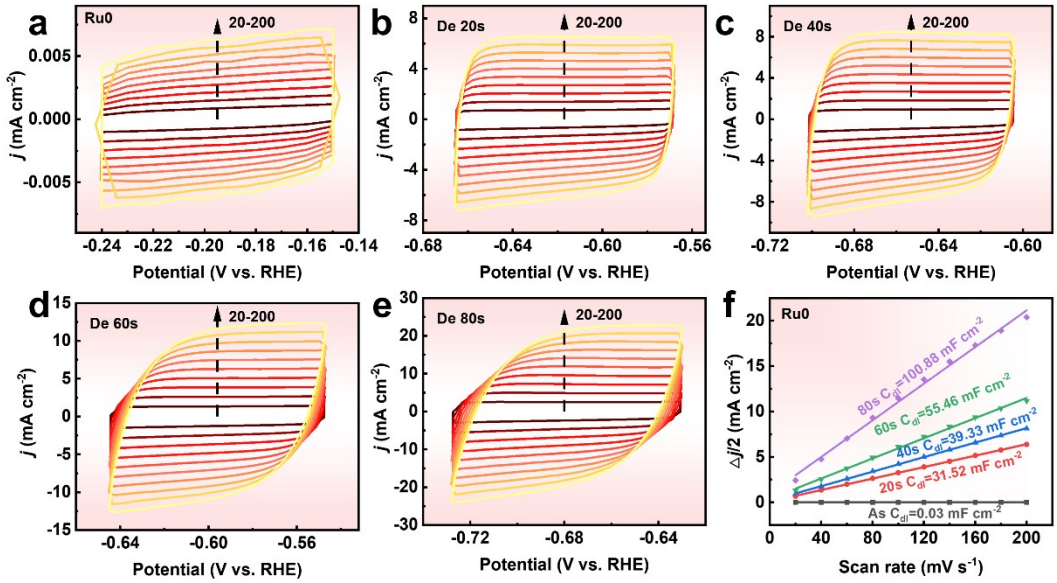

Fig. S15 Cyclic voltammogram (CV) curves in 1 M KOH for (a) Ru0, (b) Ru0-De 20s, (c) Ru0-De 40s, (d) Ru0-De 60s, (e) Ru0-De 80s. (f) Capacitive current as a function of scan rates.

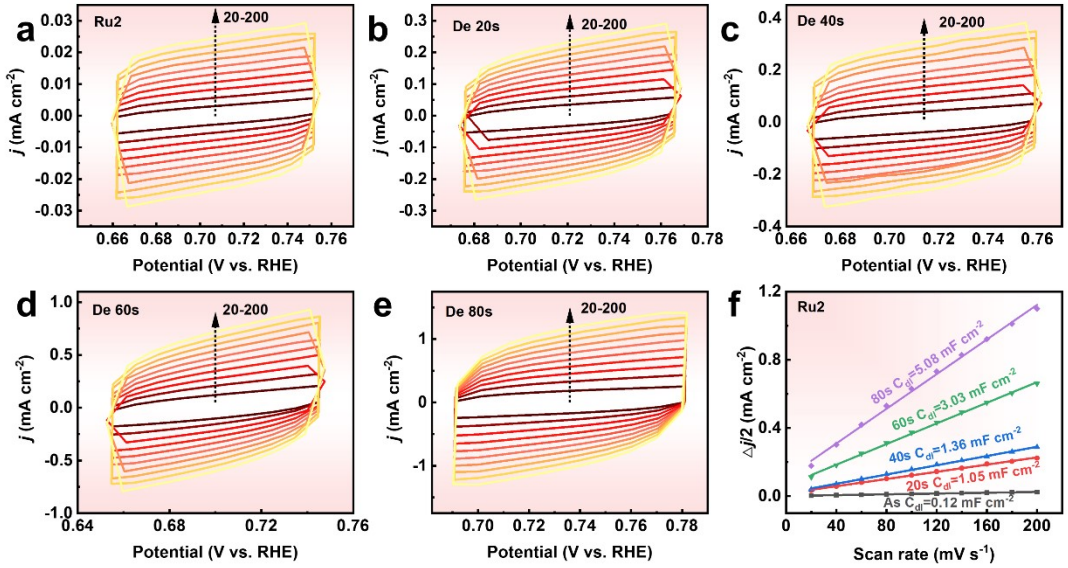

Fig. S16 Cyclic voltammogram (CV) curves in 1 M KOH for (a) Ru2, (b) Ru2-De 20s, (c) Ru2-De 40s, (d) Ru2-De 60s, (e) Ru2-De 80s. (f) Capacitive current as a function of scan rates.

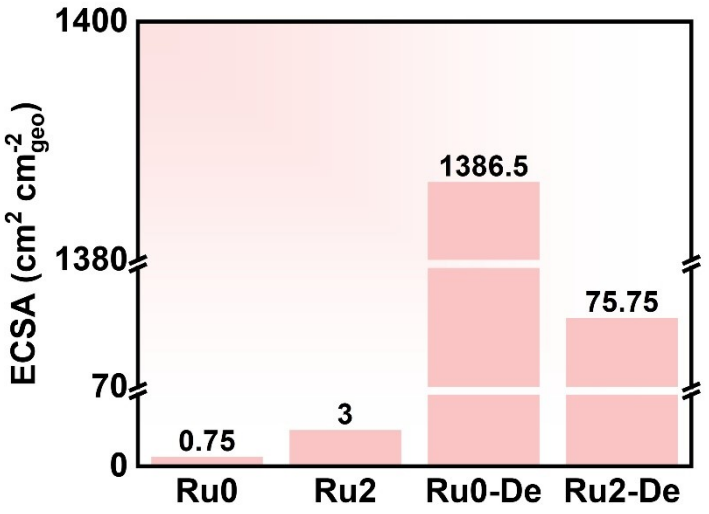

Fig. S17 Comparison of the electrochemical active specific surface area of Ru0, Ru0-De, Ru2 and Ru2-De.

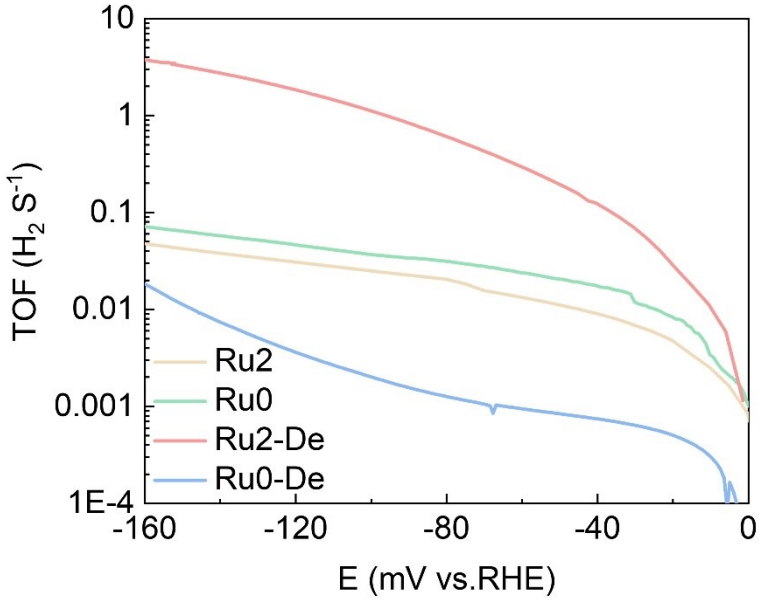

Fig. S18 TOF curves of Ru2, Ru0, Ru2-De, and Ru0-De.

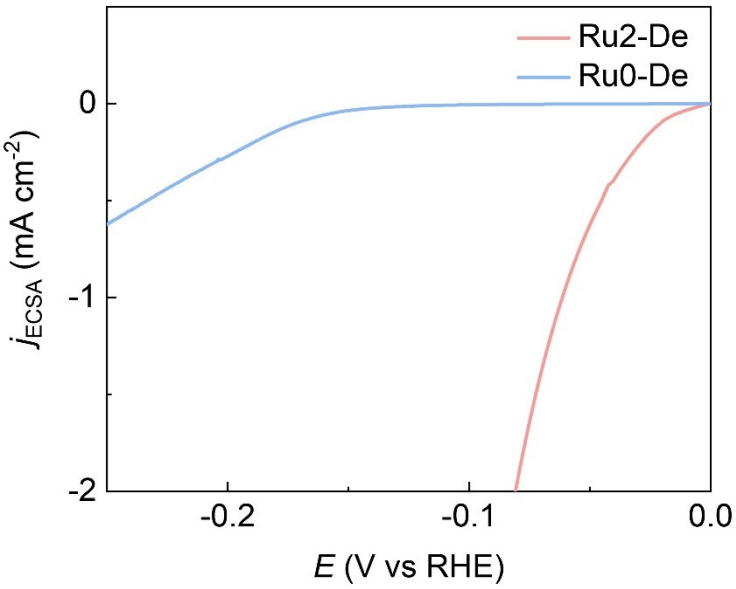

Fig. S19 Normalized polarization curves of Ru2-De and Ru0-De.

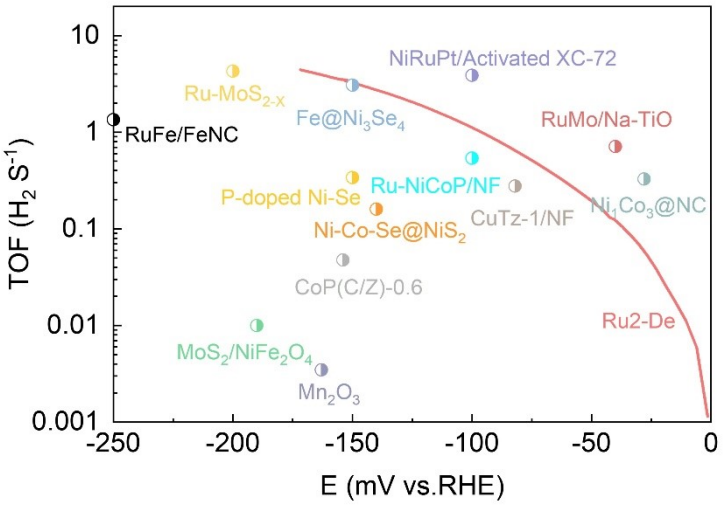

Fig. S20 Comparison of the TOF of Ru2-De catalyst with the recently reported state-of-the-art catalysts.

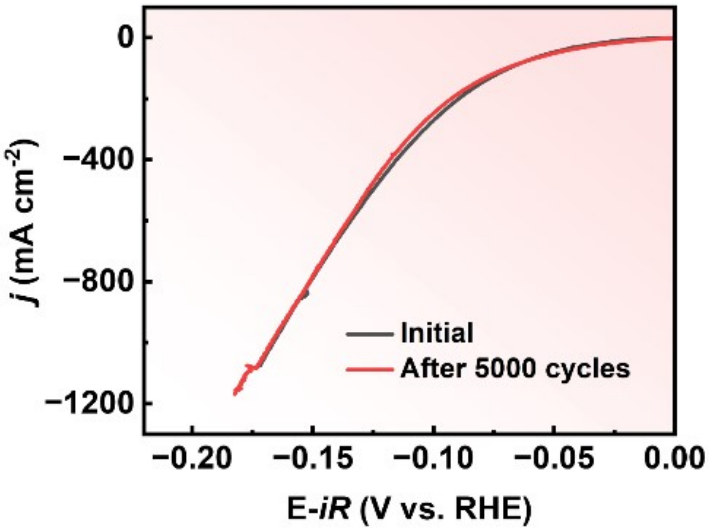

Fig. S21 Comparison of polarization curves of Ru2-De catalyst after 5000 CV cycles.

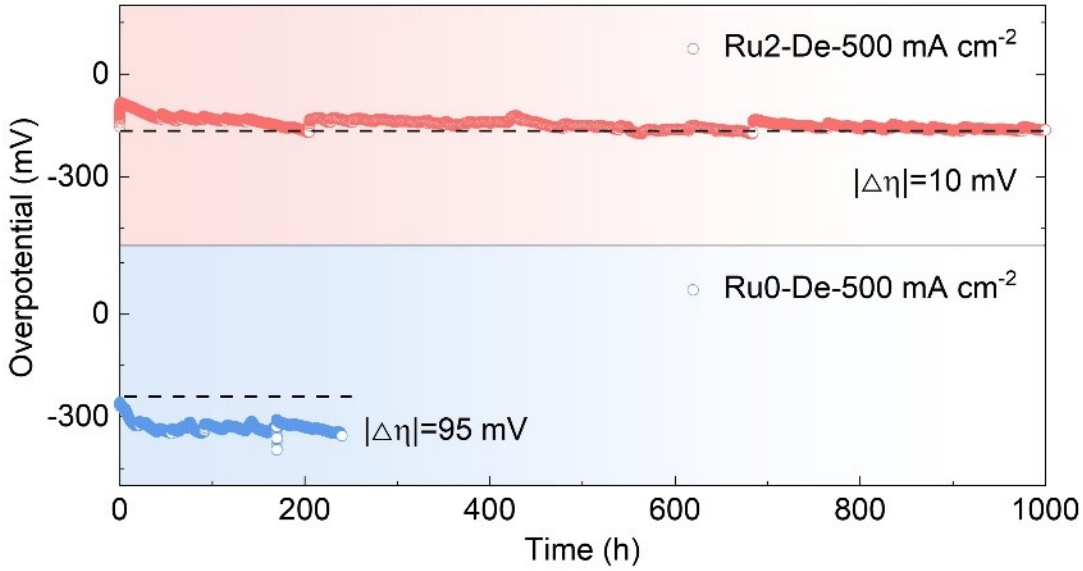

Fig. S22 Long-term stability tests of Ru0-De and Ru2-De electrodes at cathode under a constant current density of 500 mA cm^{-2}.

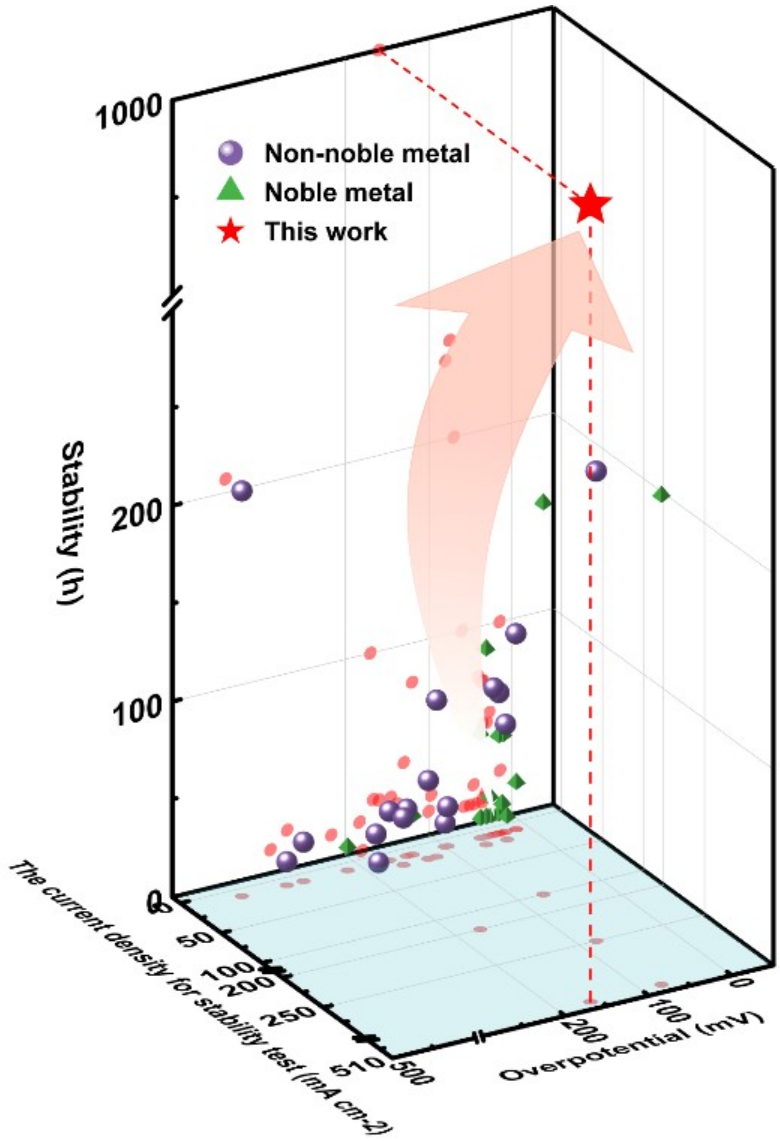

Fig. S23 Comparison of HER activity and stability with recently reported electrocatalysts.

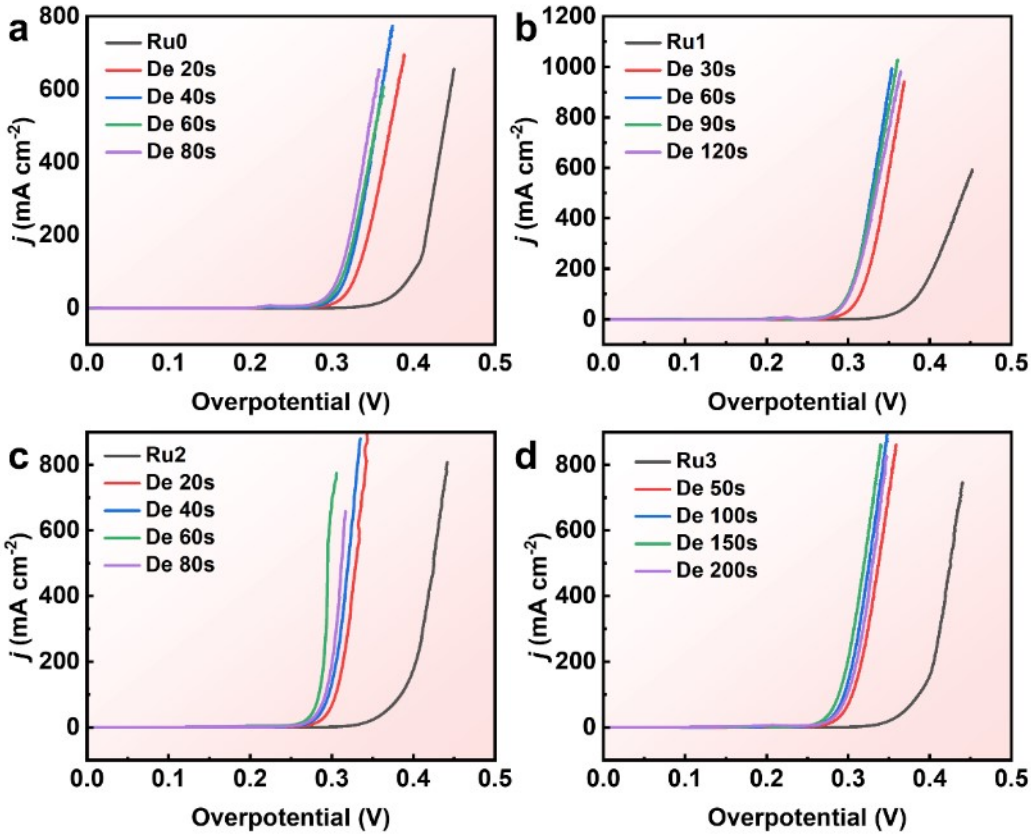

Fig. S24 OER polarization curves of dealloyed samples. (a) Ru0, (b) Ru1, (c) Ru2 and (d) Ru3.

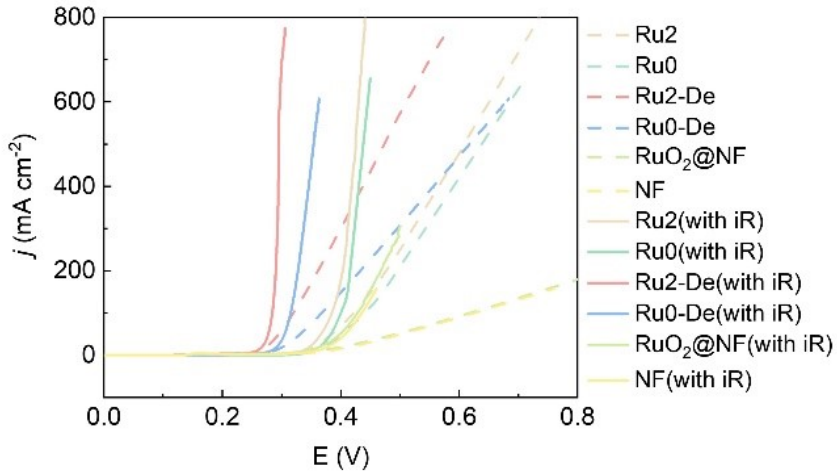

Fig. S25 OER polarization curves of different catalysts (including before and after iR compensation, 95% iR compensation).

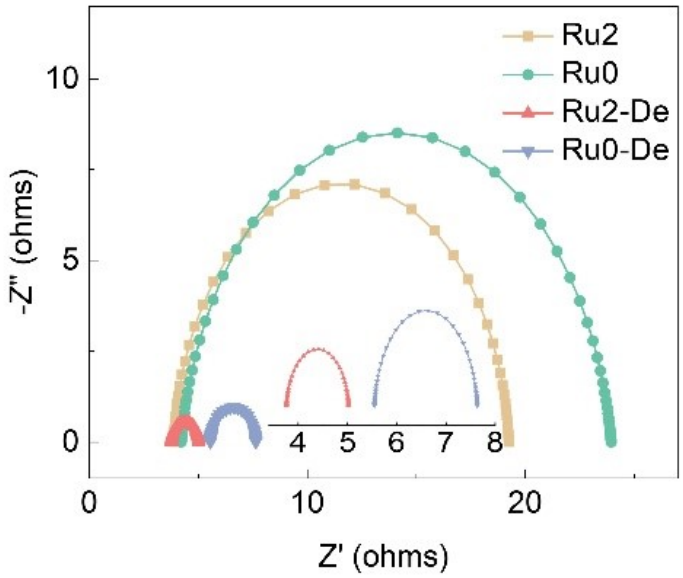

Fig. S26 EIS Nyquist plots for OER.

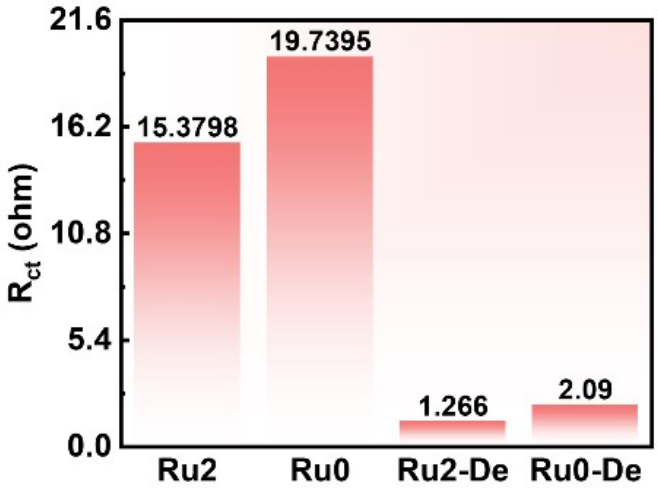

Fig. S27 Comparison of the OER electrochemical transfer resistance of Ru0, Ru0-De, Ru2 and Ru2-De.

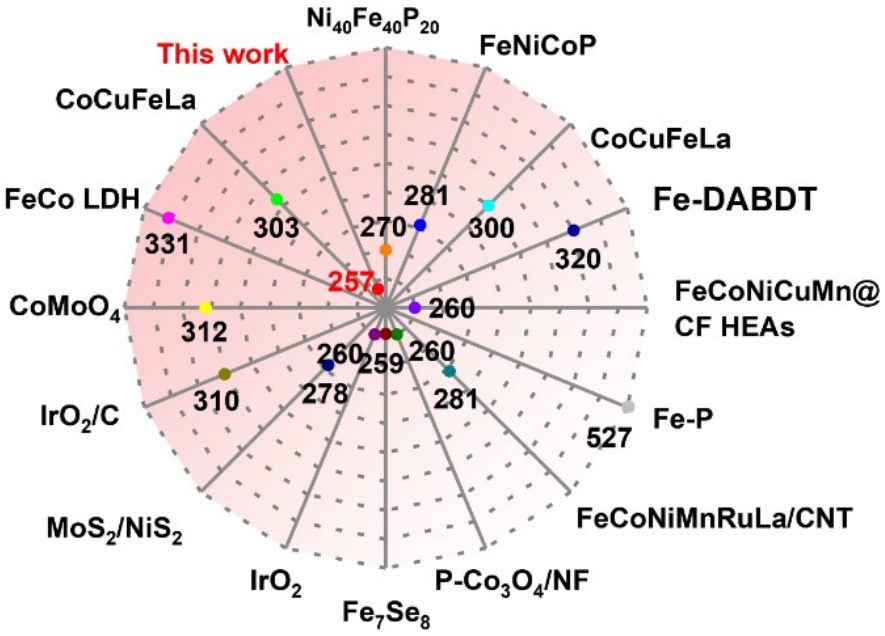

Fig. S28 Comparison of OER activity with recently reported electrocatalysts.

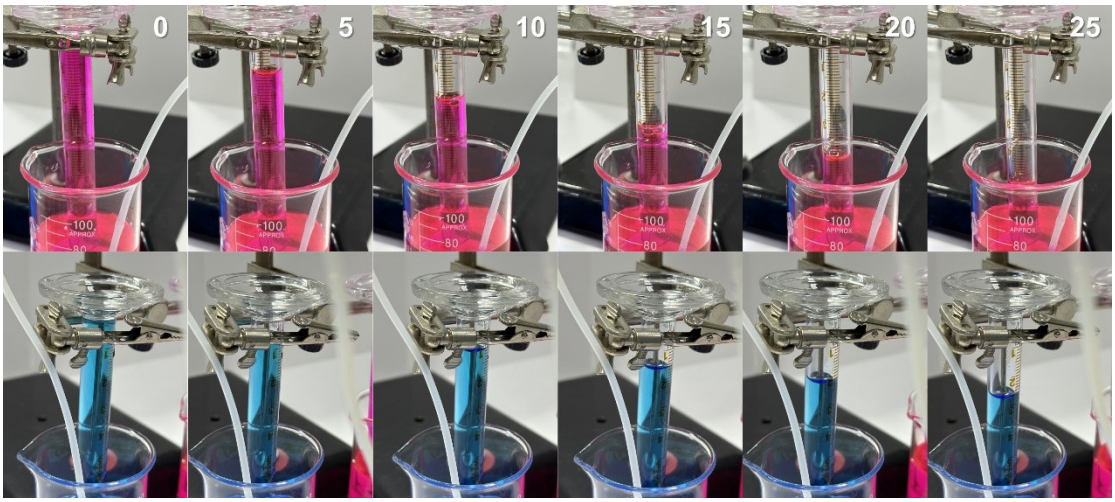

Fig. S29 Faradaic efficiency experiment of overall water splitting.

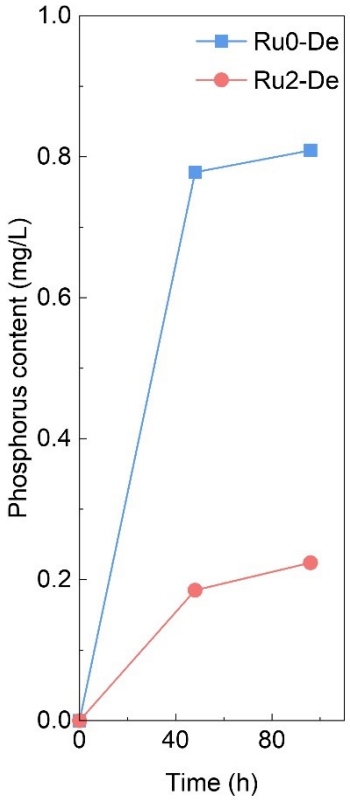

Fig. S30 Inductively coupled plasma optical emission spectroscopy (ICP-OES) results of Ru0-De and Ru2-De tested for 2 and 4 days at an anodic constant current density of 500mA cm^{-2}.

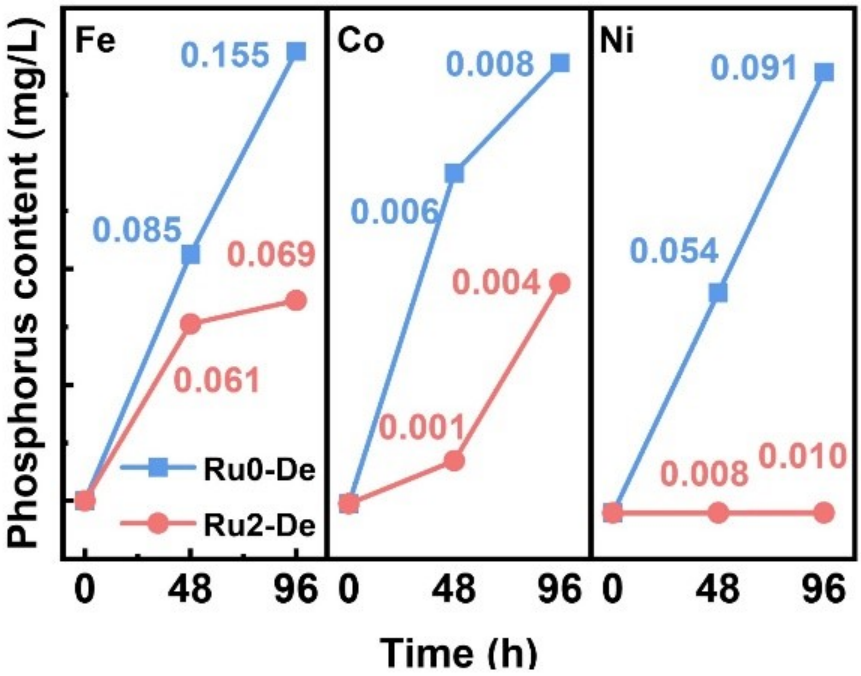

Fig. S31 ICP-OES results of Ru0-De and Ru2-De tested for 2 and 4 days at an anodic constant current density of 500mA cm^{-2}.

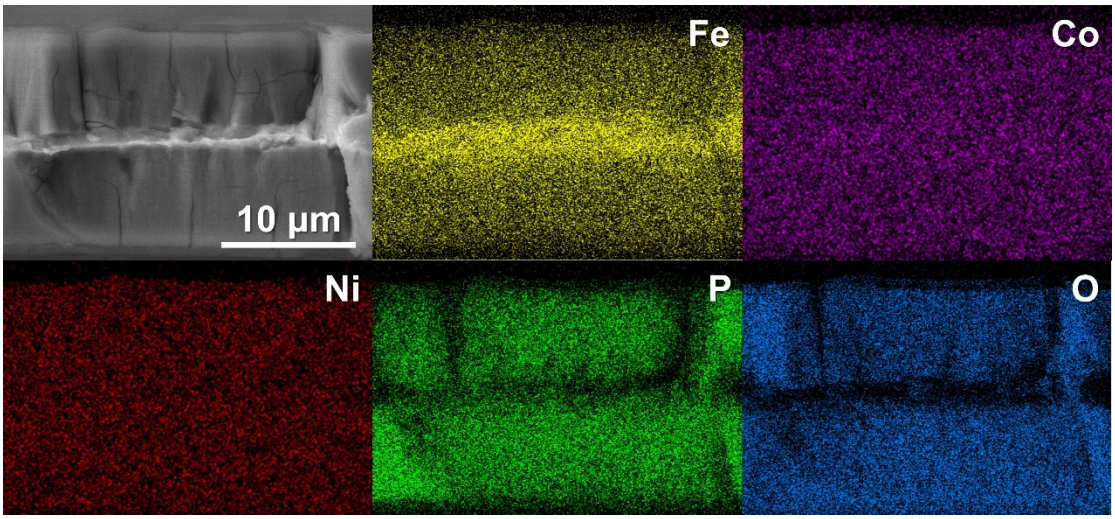

Fig. S32 Cross-sectional SEM images and EDS mapping images of Ru0-De after a 4-day constant current test at 500 mA cm^{-2}.

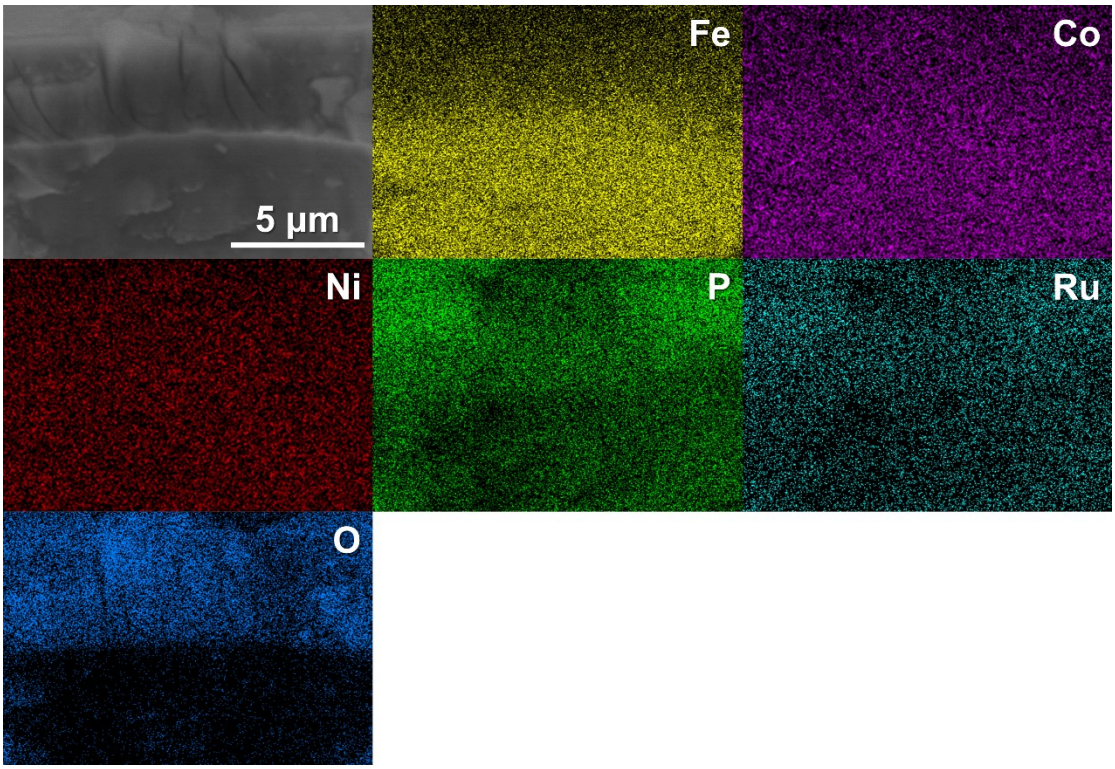

Fig. S33 Cross-sectional SEM images and EDS mapping images of Ru2-De after a 4-day constant current test at 500 mA cm^{-2}.

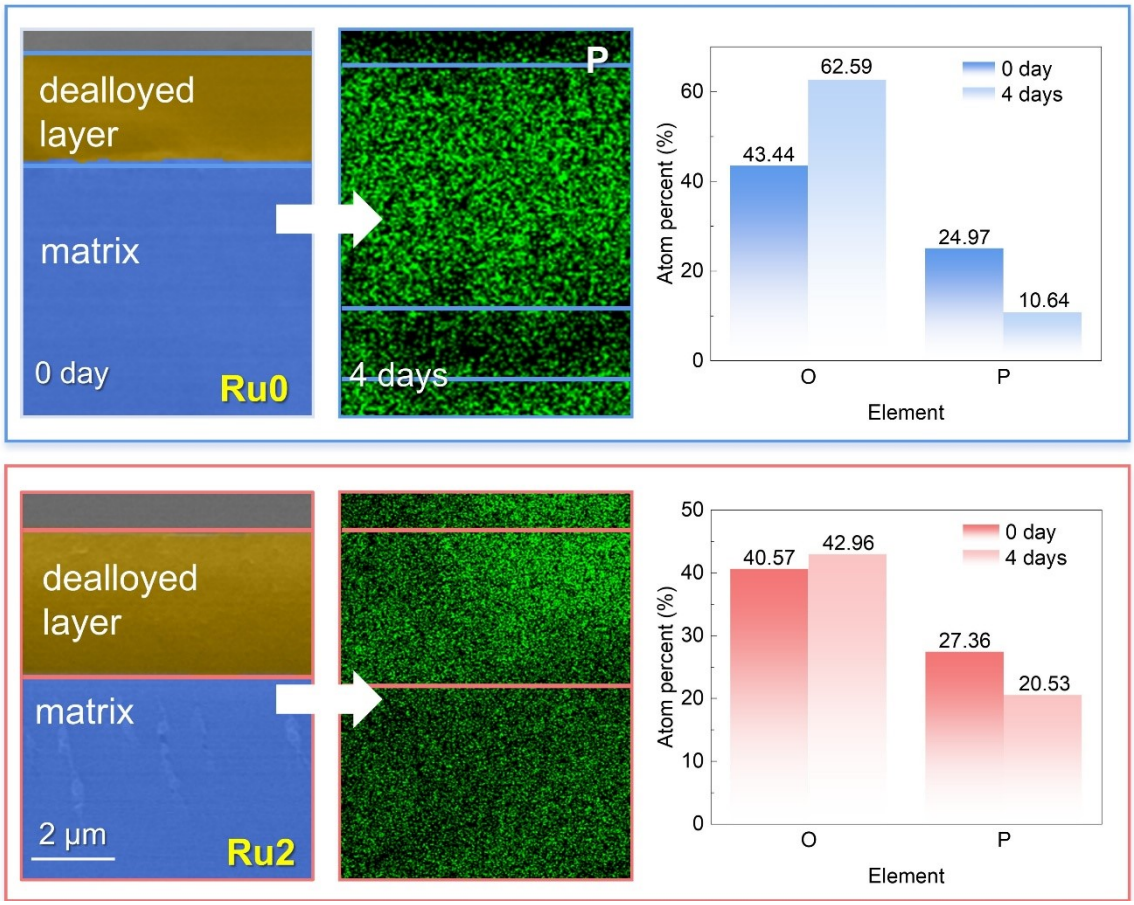

Fig. S34 Comparison of the cross-sectional SEM and EDS dealloyed layer P and O element content of the two before and after constant current testing

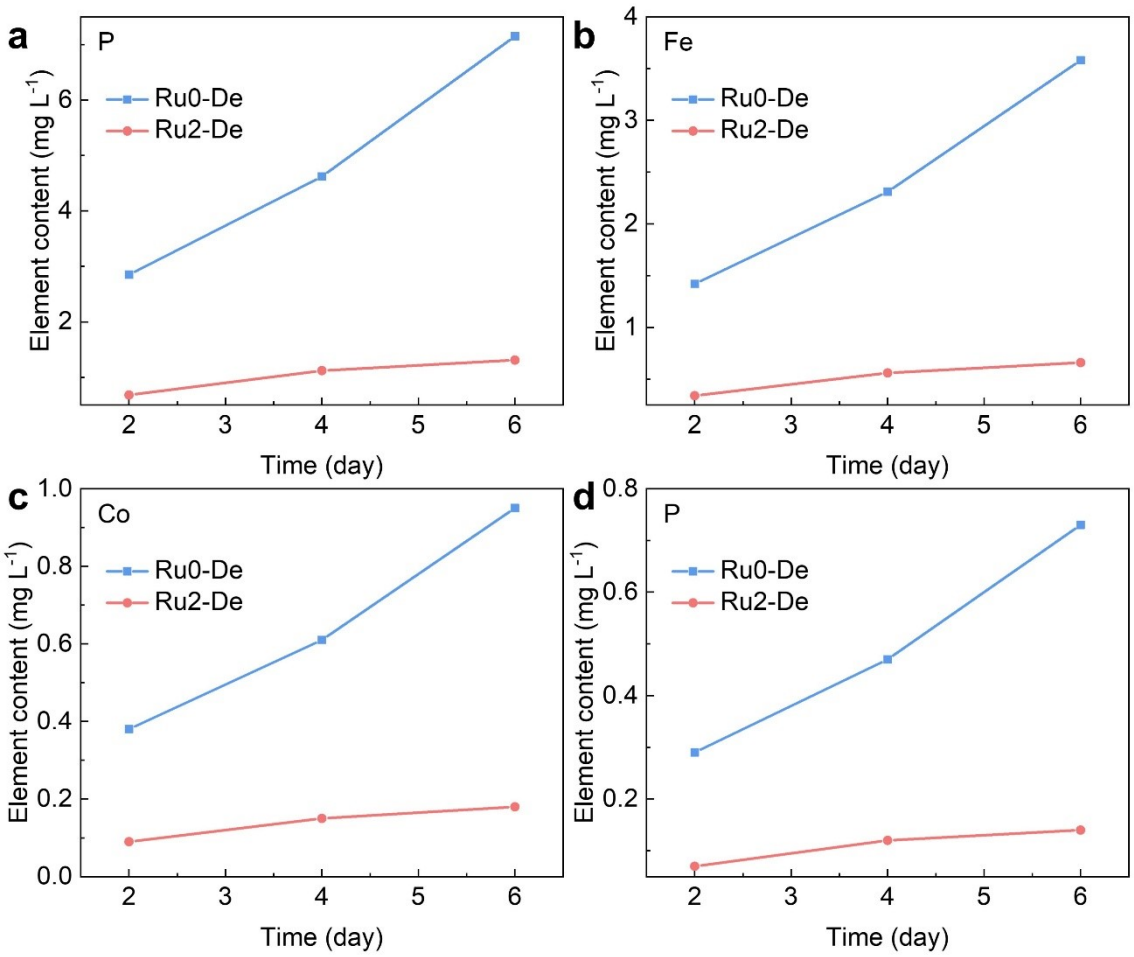

Fig. S35 ICP-OES results of Ru0-De and Ru2-De tested for 2 days, 4 days and 6 days at an anodic constant current density of 500mA cm^{-2}.

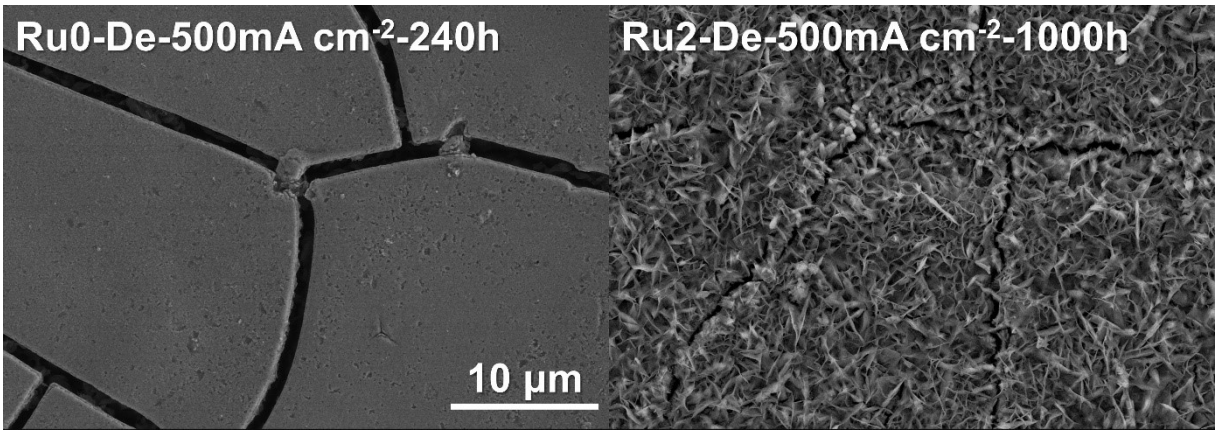

Fig. S36 SEM image after HER stability test.

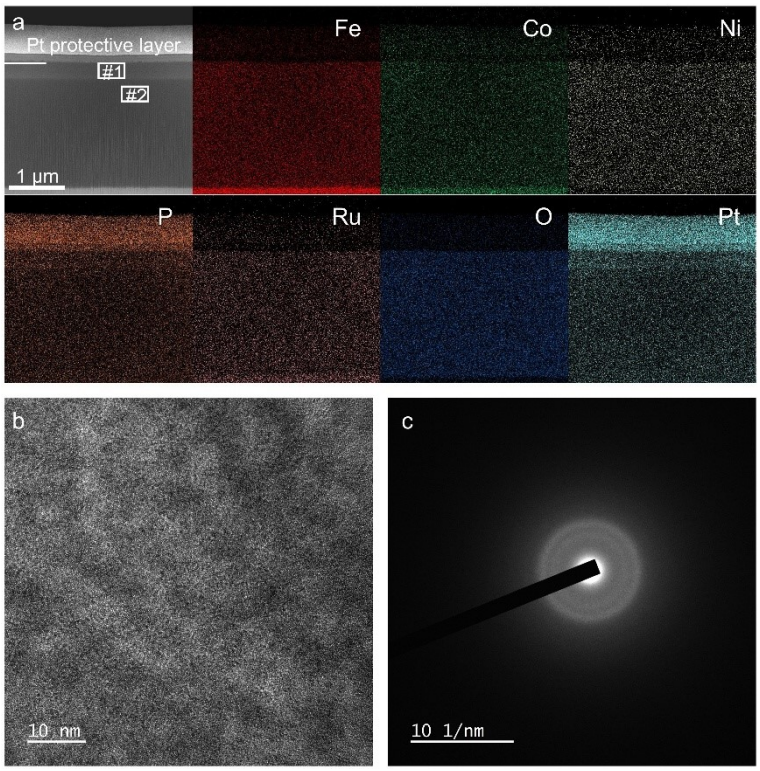

Fig. S37 HER stability test after (a) cross-sectional EDS surface scan, (b) HRTEM image, (c) SAED pattern.

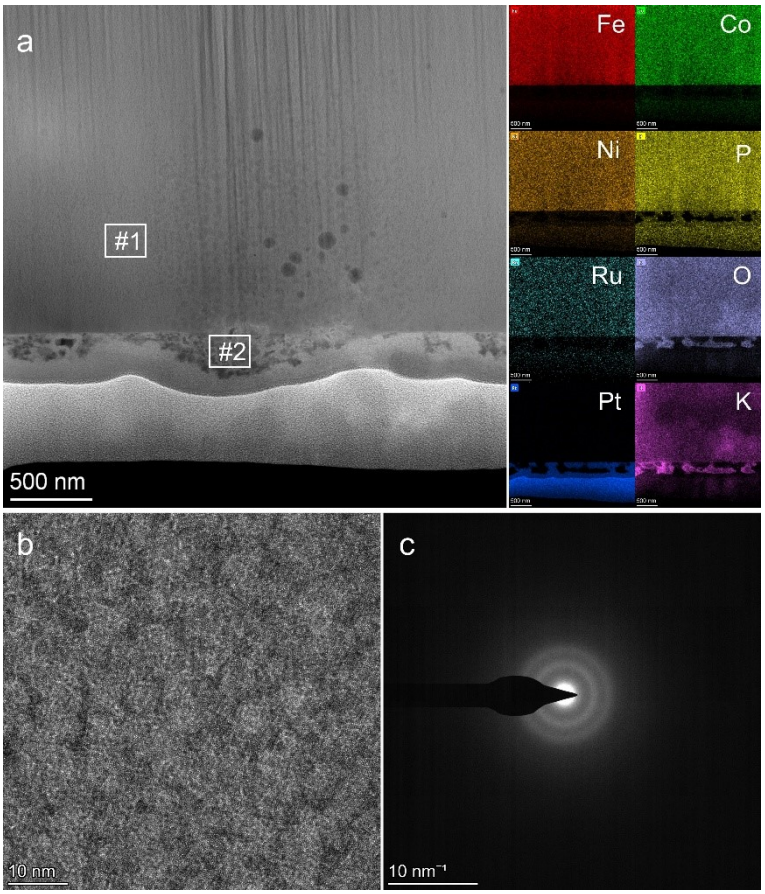

Fig. S38 OER stability test after (a) cross-sectional EDS surface scan, (b) HRTEM image, (c) SAED pattern.

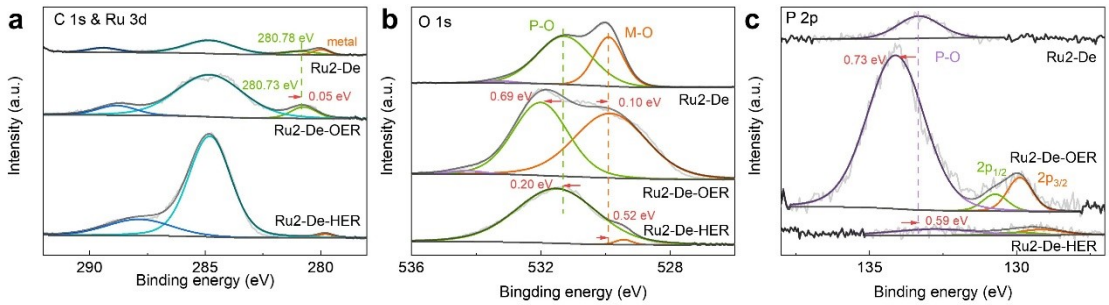

Fig. S39 Comparison of (a) Ru 3d, (b) O 1s, and (c) P 2p XPS fine spectra of Ru2-De before and after the stability test.

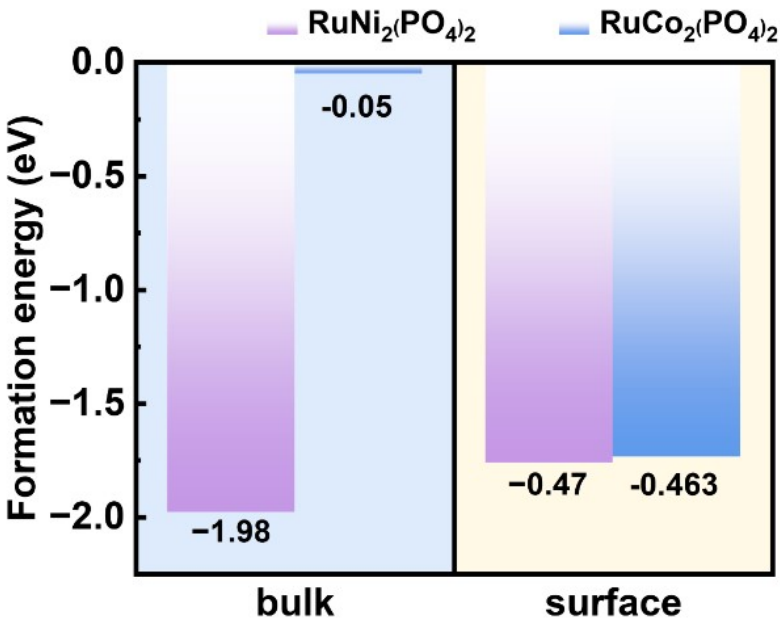

Fig. S40 Formation energy of the $RuNi_2(PO_4)_2$ and $RuCo_2(PO_4)_2$ phases and surfaces.

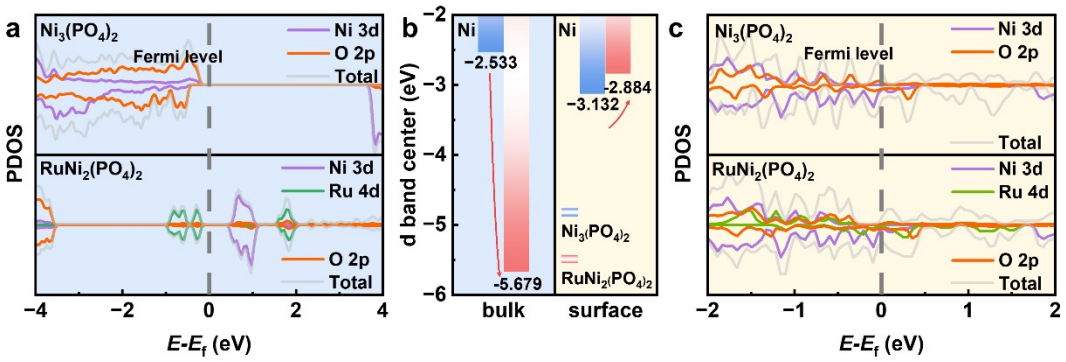

Fig. S41 Comparison of the bulk and surface PDOS of $Ni_3(PO_4)_2$ and the d-band center of Ni before and after Ru doping.

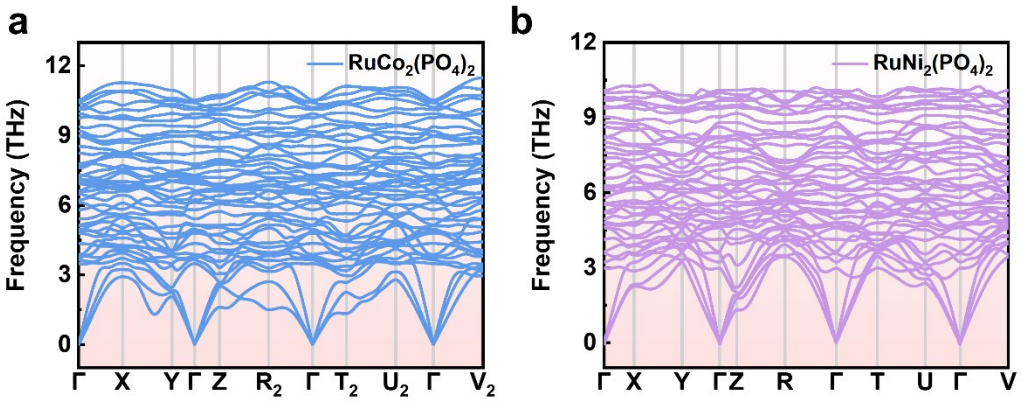

Fig. S42 Phonon spectra of $RuNi_2(PO_4)_2$ and $RuCo_2(PO_4)_2$.

Table S1. Comparison of HER performance of different electrocatalysts in alkaline media.

Catalyst	Tafel slope (mV dec^{-1})	Overpotential @10mA cm^{-2} (mV)	IR correction status	Electrolyte concentration	Temperature(℃)	Catalyst loading (mg cm^{-2})	Reference
no-noble metal							
np-CuTi	110	55	YES	0.1 M KOH	/	/	3
Ni_2P/NF	50	41	/	1 M KOH	/	/	4
Co_2P	66	183	/	1 M KOH	/	/	5
$Ni_{40}Fe_{40}P_{20}$	89	270	YES	1 M KOH	/	/	6
$P_{8.6}$-Co_3O_4/NF	86	97	/	1 M KOH	25	/	7
D15h-FeCoNiAlTi	40.1	88.2	YES	1 M KOH	/	/	8
FeCoNiMoP-S-20	57	146	/	1 M NaOH	/	/	9
Fe−Co−Ni−P−B	82.8	350	/	1 M KOH	/	/	10
Ni-Fe-Sn	98.6	27	95%	1 M KOH	25	/	11
$Ni_{46}Mn_{36}Sn_{11}Co_7$	118	290	/	1 M KOH	/	/	12
$Ni_{81}P_{19}$	69	140	YES	1 M KOH	/	/	13
$CoBO_x$/NiSe	25.5	14.5	YES	1 M KOH	/	/	14
Ni_2P/V-Pi/CC	66.5	80.8	/	1 M KOH	/	/	15
I−Ni@C	60	78	/	1 M KOH	/	0.28	16
Fe-P	102.3	436	/	1 M KOH	20	/	17
VOOH	104	164	/	1 M KOH	/	0.8	18
V/NF	82	125	95%	1 M KOH	/	/	19
$Ni_{0.75}Fe_{0.125}V_{0.125}$-LDHs/NF	62	125	/	1 M KOH	/	/	20
Ni-Fe-Sn/NF	150.8	100	/	1 M KOH	25	/	21
Ni_3Fe@BC	127	330	YES	1 M KOH	/	0.357	22
$Cu_{81}(Ni,Co)_{19}$	73.3	35	YES	1 M KOH	25	/	23
noble metal							
Pt-TiN NAs	98.3	139	/	1 M KOH	/	/	24
$(Ru-Co)O_x$	23.5	44.1	/	1 M KOH	/	/	25
FeCoNiMnRuLa/CNT	116	50	/	1 M KOH	/	1.02	26
MoP-	36.	47	95%	1 M KOH	/	/	27

Ru_2P/NPC	93						
Ru_2P@PNC/CC-900	66	50	/	1 M KOH	/	/	[28]
$Ru_{0.33}Se$@TNA	50	57	0.9	1 M KOH	25	0.2	[29]
Pt_1/N-C	36.8	46	/	1 M KOH	25	0.25	[30]
Ni-Fe-Pt NCs	81	463	/	1 M KOH	25	0.141	[31]
H-INT	38	48	/	1 M KOH	25	/	[32]
Ru/C_3N_4/C	69	79	YES	0.1M KOH	25	0.204	[33]
Pt Ni	74	65	YES	0.1M KOH	20	0.076	[34]
RuO_2/Co_3O_4	91	89	NO	1 M KOH	25	0.285	[35]
β -Ni$(OH)_2$/Pt	42	92	YES	0.1M KOH	25	0.013	[36]
Ni_3N/Pt	36.5	50	0.8	1 M KOH	25	/	[37]
Sr_2RuO_4	51	61	YES	1 M KOH	25	0.464	[38]
1D-RuO_2-CNx	70	95	YES	0.5M KOH	25	0.17	[39]
Ru_3Sn_7	40	27	YES	1M KOH	25	0.707	[40]
Ru NPs/TiN	41.4	28	YES	1M KOH	25	/	[41]
$Ni_{40}Zr_{40}Ti_{17}Pt_3$	30	37	/	1M KOH	25	/	[2]
$Al_{82}Ni_6Co_3Mn_3Y_3Au_3$	43	24	YES	1M KOH	25	/	[42]
PdPtCuNiP	37.4	32	YES	1M KOH	25	/	[43]
Ru2	92.7	299	0.95	1 M KOH	25	10.67	This work
Ru2-De	30.74	23	0.95	1 M KOH	25	/	This work

Table S2. Comparison of the TOF of Ru2-De catalyst with the recently reported state-of-the-art catalysts.

Electrocatalysts	Overpotential(mV)	TOF(H_2 S^{-1})	Refs.
CoP(C/Z)-0.6	154	0.0477	[44]
Ni_1Co_3@NC	28	0.328	[45]
Ru-NiCoP/NF	100	0.54	[46]
Ru-MoS_{2-x}	200	4.29	[47]
RuFe/FeNC	250	1.35	[48]
CuTz-1/NF	82	0.277	[49]
NiRuPt/Activated XC-72	100	3.88	[50]
RuMo/Na-TiO	40	0.71	[51]
Ni-Co-Se@NiS_2	140	0.16	[52]
MoS_2/$NiFe_2O_4$	190	0.01	[53]
Mn_2O_3	163	0.00347	[54]
P-doped Ni-Se	150	0.339	[55]
Fe@Ni_3Se_4	150	3.07	[56]
Ru2-De	100	1.12	This work

Table S3. Comparison of HER stability of different electrocatalysts in alkaline media.

Catalyst	The current density for stability test (mA cm^{-2})	Overpotential (mV)	Stability（h）	Reference
Ni_2P/Ni	10	41	75	4
Co_2P	10	183	15	5
$Ni_{40}Fe_{40}P_{20}$	10	270	20	6
Pt-TiN NAs	10	139	20	24
$P_{8.6}$-Co_3O_4/NF	10	97	20	7
$Pd_{45}Cu_{39}Ru_{16}$/C-450	10	31	15	57
Ru-MnFeP/NF	10	35	50	58
（Ru-Co）O_x	10	44.1	10	25
PdPtCuNiP	20	60	100	43
FeCoNiMoP-S-20	10	146	24	9
$Al_{82}Ni_6Co_3Mn_3Y_3Au_3$	20	35	12	42
Ni-Fe-Sn/NF	10	100	12	21
Ni-Fe-Sn	10	27	55	11
$CoBO_x$/NiSe	10	14.5	100	14
NiFeCoCuTi	250	80	240	59
$Ti_{37}Cu_{60}Ru_3$	10	35	10	60
Ru_3Sn_7	10	30	50	40
$Ru_{0.48}Re_{0.52}$NPs@rGO	10	14	24	61
$(FeCoNiB_{0.75})_{97}Pt_3$	100	70	200	62
I−Ni@C	20	120	80	16
$Cu_{81}(Ni,Co)_{19}$	10	35	72	23
Fe-P	10	436	207	17
VOOH	10	167	25	18
V/NF	20	160	24	19
D15h HEIs	20	130	40	8
$Ni_{46}Mn_{36}Sn_{11}Co_7$	10	290	12	12
$Ni_{81}P_{19}$	10	180	0.17	13
Ru/ac-$CeO_{2-\delta}$	200	170	100	63
$Ni_{40}Zr_{40}Ti_{17}Pt_3$	10	37	72	2
$Fe_{67}Co_{10}Ni_{10}Zr_{10}Pt_3$	500	75	250	64
MoP-Ru_2P/NPC	10	217	12	27
Ru_2P@PNC/CC-900	10	50	10	28
$Ru_{0.33}Se$@TNA	10	57	10	29
Pt_1/N-C	10	46	20	30
Ru2-De	500	177	1000	This work

Table S4. Comparison of OER performance of different electrocatalysts in alkaline media.

Catalyst	Tafel slope (mV dec^{-1})	Overpotential @10mA cm^{-2} (mV)	IR correction status	Electrolyte concentration	Temperature(℃)	Catalyst loading(mg cm^{-2})	Reference
$Ni_{40}Fe_{40}P_{20}$	35	270	YES	1 M KOH	/	/	6
FeNiCoP	38	281	YES	1M NaOH	25	/	65
CoCuFeLa	105.04	300	YES	1M KOH	25	0.5	66
Fe-DABDT	72.2	320	YES	1M KOH	25	/	67
FeCoNiCuMn @CF HEAs	28	260	/	1M KOH	25	19.8	68
Fe-P	77.2	527	/	1 M KOH	20	/	17
FeCoNiMnRuLa/CNT	47.5	281	/	1 M KOH	/	1.02	26
P-Co_3O_4/NF	60	260	/	1 M KOH	25	/	7
Fe_7Se_8	76.6	259	/	1M KOH	25	/	69
IrO_2	45	260	0.95	0.1M KOH	25	/	70
MoS_2/NiS_2	91.7	278	YES	1M KOH	25	/	71
IrO_2/C	84.4	310	YES	1M KOH	25	0.2	72
$CoMoO_4$	56	312	NO	1M KOH	25	0.1	73
FeCo LDH	85	331	0.95	1M KOH	25	0.21	74
As-Ru2	92.7	299	0.95	1 M KOH	25	10.67	This work
Ru2-De	30.74	23	0.95	1 M KOH	25	/	This work

Table S5. Comparison of OWS performance of different electrocatalysts in alkaline media.

Catalyst	Overall water splitting @500mA cm^{-2} (V)	Electrolyte	Reference
Ni_2P-Fe_2P/NF	1.865	1 M KOH	[75]
NiCoP/NF	1.83	1 M KOH	[76]
Fe_2P/Co_2N	1.663	1 M KOH	[77]
NiCo(nf)-P	1.86	1 M KOH	[78]
Ru-CMOP	1.828	1 M KOH	[79]
NiCoP-2/NF	2.13	1 M KOH	[80]
$NiCo_3P$.C/NF	2.6	1 M KOH	[81]
W/NiB	1.85	1 M KOH	[82]
CrP-Re_2P	1.89	1 M KOH	[83]
NiCoMoO	1.95	1 M KOH	[84]
Fe/Ni_2P	1.78	1 M KOH	[85]
$(Fe,Ni)_2P$	1.88	1 M KOH	[86]
MnO/NiFeP	1.79	1 M KOH	[87]
MnO/NiFeP	1.87	1 M KOH	[88]
FeCoNi	1.87	1 M KOH	[89]
Ni-FeSx/NiFe	2.6	1 M KOH	[90]
Ni_2P/FeP	2.39	1 M KOH	[91]
Co-Mn-B	2.1	1 M KOH	[92]
NiMoB	2.2	1 M KOH	[93]
Ni_2P/CoP-NF	1.91	1 M KOH	[94]
Ru,Fe-Ni_5P_4/C	1.872	1 M KOH	[95]
3D RuCoP/NF	1.82	1 M KOH	[96]
Ru/CuMnBP	2.03	1 M KOH	[97]
Ru-NiCoP@NF	~1.78	1 M KOH	[98]
Ru0-De	1.79	1 M KOH	This work
Ru2-De	1.7	1 M KOH	This work

Reference

1. Z. Jia, Y. Zhao, Q. Wang, F. Lyu, X. Tian, S.-X. Liang, L.-C. Zhang, J. Luan, Q. Wang, L. Sun, T. Yang and B. Shen, ACS Applied Materials & Interfaces, 2022, 14, 10288-10297.
2. R. Li, X. Liu, R. Wu, J. Wang, Z. Li, K. C. Chan, H. Wang, Y. Wu and Z. Lu, Advanced Materials, 2019, 31, 1904989.
3. Q. Lu, G. S. Hutchings, W. Yu, Y. Zhou, R. V. Forest, R. Tao, J. Rosen, B. T. Yonemoto, Z. Cao, H. Zheng, J. Q. Xiao, F. Jiao and J. G. Chen, Nature Communications, 2015, 6.
4. Y. Shi, Y. Xu, S. Zhuo, J. Zhang and B. Zhang, ACS Applied Materials & Interfaces, 2015, 7, 2376-2384.
5. C. G. Read, J. F. Callejas, C. F. Holder and R. E. Schaak, ACS Applied Materials & Interfaces, 2016, 8, 12798-12803.
6. Y. Tan, F. Zhu, H. Wang, Y. Tian, A. Hirata, T. Fujita and M. Chen, Advanced Materials Interfaces, 2017, 4, 1601086.
7. Z. Wang, H. Liu, R. Ge, X. Ren, J. Ren, D. Yang, L. Zhang and X. Sun, ACS Catalysis, 2018, 8, 2236-2241.
8. Z. Jia, T. Yang, L. Sun, Y. Zhao, W. Li, J. Luan, F. Lyu, L. C. Zhang, J. J. Kruzic, J. J. Kai, J. C. Huang, J. Lu and C. T. Liu, Advanced Materials, 2020, 32.
9. S. Jiang, L. Zhu, Z. Yang and Y. Wang, Electrochimica Acta, 2021, 389.
10. L. Cai, J. Huo, P. Zou, G. Li, J. Liu, W. Xu, M. Gao, S. Zhang and J.-Q. Wang, ACS Applied Materials & Interfaces, 2022, 14, 15243-15249.
11. S. You, Y. Wu, Y. Wang, Z. He, L. Yin, Y. Zhang, Z. Sun and Z. Zhang, International Journal of Hydrogen Energy, 2022, 47, 29315-29326.
12. Z. Fan, P. Zou, K. Jiang, W. Xu, M. Gao, V. Zadorozhnyy, G. Li, J. Huo and J.-Q. Wang, Intermetallics, 2023, 160.
13. I. Flis-Kabulska and J. Flis, ChemElectroChem, 2023, 10.
14. Y. Liu, T. Sakthivel, F. Hu, Y. Tian, D. Wu, E. H. Ang, H. Liu, S. Guo, S. Peng and Z. Dai, Advanced Energy Materials, 2023, 13.
15. J. Fan, L. Wang, X. Xiang, Y. Liu, N. Shi, Y. Lin, D. Xu, J. Jiang, Y. Lai, J. Bao and M. Han, Small Methods, 2024, 8.
16. C. Liu, B. Sheng, Q. Zhou, Y. Xia, Y. Zou, P. J. Chimtali, D. Cao, Y. Chu, S. Zhao, R. Long, S. Chen and L. Song, Journal of the American Chemical Society, 2024, 146, 26844-26854.
17. T. Zhang, X. Ren, S. Mo, W. Cao, C. Zhou, F. Ma, R. Chen, C. Zeng, L. Shi, T. Liu, H. Zhang and H. Ni, Journal of Materials Science & Technology, 2024, 199, 66-74.
18. H. Shi, H. Liang, F. Ming and Z. Wang, Angewandte Chemie International Edition, 2016, 56, 573-577.
19. Y. Yu, P. Li, X. Wang, W. Gao, Z. Shen, Y. Zhu, S. Yang, W. Song and K. Ding, Nanoscale, 2016, 8, 10731-10738.
20. K. N. Dinh, P. Zheng, Z. Dai, Y. Zhang, R. Dangol, Y. Zheng, B. Li, Y. Zong and Q. Yan, Small, 2017, 14.
21. Y. Wu, Y. Zhang, Y. Wang, Z. He, Z. Gu and S. You, International Journal of Hydrogen Energy, 2021, 46, 26930-26939.
22. Y. B. Adegbemiga, N. Ullah, M. Xie, S. Hussain, C. J. Oluigbo, W. Yaseen, A. J. Kumar, Y. Xu and J. Xie, Journal of Alloys and Compounds, 2020, 835.
23. C. Wang, P. Zou, W. Xu, Y. Zhang, J. Huo, J.-Q. Wang, Y. Liu and C. Qin, Journal of Alloys and Compounds, 2024, 995, 174790.
24. C. Wang, H. Shi, H. Liu, J. Fu, D. Wei, W. Zeng, Q. Wan, G. Zhang and H. Duan, Electrochimica Acta, 2018, 292, 727-735.
25. C. Wang and L. Qi, Angewandte Chemie International Edition, 2020, 59, 17219-17224.
26. Z.-L. Wang, G.-Y. Huang, G.-R. Zhu, H.-C. Hu, C. Li, X.-H. Guan and H.-B. Zhu, Applied

Catalysis B: Environment and Energy, 2025, 361.
27.Y. Gao, Z. Chen, Y. Zhao, W. Yu, X. Jiang, M. He, Z. Li, T. Ma, Z. Wu and L. Wang, Applied Catalysis B: Environmental, 2022, 303.
28.T. Liu, B. Feng, X. Wu, Y. Niu, W. Hu and C. M. Li, ACS Applied Energy Materials, 2018, 1, 3143-3150.
29.K. Wang, Q. Chen, Y. Hu, W. Wei, S. Wang, Q. Shen and P. Qu, Small, 2018, 14.
30.S. Fang, X. Zhu, X. Liu, J. Gu, W. Liu, D. Wang, W. Zhang, Y. Lin, J. Lu, S. Wei, Y. Li and T. Yao, Nature Communications, 2020, 11.
31.M. Fu, Q. Zhang, Y. Sun, G. Ning, X. Fan, H. Wang, H. Lu, Y. Zhang and H. Wang, International Journal of Hydrogen Energy, 2020, 45, 20832-20842.
32.D. Liu, Z. Song, S. Cheng, Y. Wang, A. Saad, S. Deng, J. Shen, X. Huang, X. Cai and P. Tsiakaras, Chemical Engineering Journal, 2022, 431.
33.Y. Zheng, Y. Jiao, Y. Zhu, L. H. Li, Y. Han, Y. Chen, M. Jaroniec and S.-Z. Qiao, Journal of the American Chemical Society, 2016, 138, 16174-16181.
34.Z. Cao, Q. Chen, J. Zhang, H. Li, Y. Jiang, S. Shen, G. Fu, B.-a. Lu, Z. Xie and L. Zheng, Nature Communications, 2017, 8.
35.H. Liu, G. Xia, R. Zhang, P. Jiang, J. Chen and Q. Chen, RSC Advances, 2017, 7, 3686-3694.
36.X. Yu, J. Zhao, L.-R. Zheng, Y. Tong, M. Zhang, G. Xu, C. Li, J. Ma and G. Shi, ACS Energy Letters, 2017, 3, 237-244.
37.Y. Wang, L. Chen, X. Yu, Y. Wang and G. Zheng, Advanced Energy Materials, 2016, 7.
38.Y. Zhu, H. A. Tahini, Z. Hu, J. Dai, Y. Chen, H. Sun, W. Zhou, M. Liu, S. C. Smith, H. Wang and Z. Shao, Nature Communications, 2019, 10.
39.T. Bhowmik, M. K. Kundu and S. Barman, ACS Applied Materials & Interfaces, 2016, 8, 28678-28688.
40.Z. Wang, Z. Lin, Y. Wang, S. Shen, Q. Zhang, J. Wang and W. Zhong, Advanced Materials, 2023, 35.
41.J. Zhao, R. Urrego-Ortiz, N. Liao, F. Calle-Vallejo and J. Luo, Nature Communications, 2024, 15, 6391.
42.X. Liu, S. Ju, P. Zou, L. Song, W. Xu, J. Huo, J. Yi, G. Wang and J.-Q. Wang, Journal of Alloys and Compounds, 2021, 880.
43.Z. Jia, K. Nomoto, Q. Wang, C. Kong, L. Sun, L. C. Zhang, S. X. Liang, J. Lu and J. J. Kruzic, Advanced Functional Materials, 2021, 31.
44.Y.-L. Meng, J. Tang, X. Chen, Z.-Y. Niu, Y.-H. Zhao, Y. Pan, X.-F. Wang, X.-Z. Song and Z. Tan, Inorganic Chemistry Communications, 2021, 134.
45.B. Mohanty, L. Pradhan, B. Satpati, P. Rajput, M. Ghorbani-Asl, Y. Wei, P. W. Menezes, A. V. Krasheninnikov and B. K. Jena, Journal of Power Sources, 2025, 625.
46.Y. Guo, G. Zhou and Y. Tong, Dalton Transactions, 2023, 52, 12733-12741.
47.X.-Y. Li, S.-J. Zhu, Y.-L. Wang, T. Lian, X.-y. Yang, C.-F. Ye, Y. Li, B.-L. Su and L.-H. Chen, Frontiers in Chemistry, 2022, 10.
48.Q. He, Y. Zhou, L. Mou, C. Wu, D. Liu, B. Ge, J. Jiang and L. Song, Energy & Environmental Science, 2025, 18, 1984-1991.
49.M. I. Anwar, T. Wang, M. Asad, K. Jabbour, S. Manzoor, L. Ma, N. Ahmed, W. Zhang, M. N. Ashiq and G. Yang, International Journal of Hydrogen Energy, 2024, 51, 242-255.
50.T. T. Huynh, V. T. T. Mai, A. Q. K. Nguyen and H. Q. Pham, Advanced Sustainable Systems, 2023, 8.
51.G. Lin, Q. Ju, L. Liu, X. Guo, Y. Zhu, Z. Zhang, C. Zhao, Y. Wan, M. Yang, F. Huang and J. Wang, ACS Nano, 2022, 16, 9920-9928.
52.S. Jamali, M. Abedini Mohammadi, M. Saghafi Yazdi, M. Talafi Noghani, A. Moghanian, M. Rezayat and M. Morales, Journal of Electroanalytical Chemistry, 2024, 969.
53.J. Xu, T. Liu, J. Li, B. Li, Y. Liu, B. Zhang, D. Xiong, I. Amorim, W. Li and L. Liu,

Energy & Environmental Science, 2018, 11, 1819-1827.
54.P. D. Sachin, S. Ashoka S and K. Yogesh, Colloids and Surfaces A: Physicochemical and Engineering Aspects, 2025, 726.
55.M. Maleki, A. Sabour Rouhaghdam, G. Barati Darband, D. Han, M. Chehelamirani and S. Shanmugam, Journal of Electroanalytical Chemistry, 2022, 916.
56.A. Karmakar, A. V. Krishnan, R. Jayan, R. Madhu, M. M. Islam and S. Kundu, Journal of Materials Chemistry A, 2023, 11, 10684-10698.
57.M. Li, M. Luo, Z. Xia, Y. Yang, Y. Huang, D. Wu, Y. Sun, C. Li, Y. Chao, W. Yang, W. Yang, Y. Yu and S. Guo, Journal of Materials Chemistry A, 2019, 7, 20151-20157.
58.D. Chen, Z. Pu, R. Lu, P. Ji, P. Wang, J. Zhu, C. Lin, H. W. Li, X. Zhou, Z. Hu, F. Xia, J. Wu and S. Mu, Advanced Energy Materials, 2020, 10.
59.H. Shi, X.-Y. Sun, S.-P. Zeng, Y. Liu, G.-F. Han, T.-H. Wang, Z. Wen, Q.-R. Fang, X.-Y. Lang and Q. Jiang, Small Structures, 2023, 4.
60.J. Tian, Y. Hu, W. Lu, J. Zhu, X. Liu, J. Shen, G. Wang and J. Schroers, Carbon Energy, 2023, 5.
61.S. Xu, P. Zhang, Z. Li, C.-H. Chung, M.-W. Moon, J. M. Kim and P. J. Yoo, Applied Surface Science, 2023, 638.
62.X. Zhang, Y. Yang, Y. Liu, Z. Jia, Q. Wang, L. Sun, L. C. Zhang, J. J. Kruzic, J. Lu and B. Shen, Advanced Materials, 2023, 35.
63.Q. Qin, H. Jang, X. Jiang, L. Wang, X. Wang, M. G. Kim, S. Liu, X. Liu and J. Cho, Angewandte Chemie International Edition, 2023, 63.
64.M. Pan, H. Feng, Z. Zhang, M. Gao, L. Lei, D. Wang, G. Li, J. Huo and J.-Q. Wang, Journal of Materials Chemistry A, 2024, 12, 15334-15342.
65.S. Jiang, L. Zhu, Z. Yang and Y. Wang, Electrochimica Acta, 2021, 368, 137618.
66.J. Feng, J. Liu, C. Chu, L. Wei, H. Li and J. Shen, Chemical Engineering Journal, 2024, 486.
67.L. Lin, Y. Xu, Y. Han, R. Xu, T. Wang, Z. Sun and Z. Yan, Journal of the American Chemical Society, 2024, 146, 7363-7372.
68.C. Yu, X.-w. Wang, W.-x. He, Z.-y. Zheng, X.-j. Dang and Y.-f. Zhang, Surfaces and Interfaces, 2024, 46.
69.C. Zhong, W. Zhou, X. Luo, T. Li, F. Huang, J. Hu, Z. Jiang, C. Hu, W. Lei and C. Yuan, Nano Letters, 2025, 25, 1550-1557.
70.D. Friebel, M. W. Louie, M. Bajdich, K. E. Sanwald, Y. Cai, A. M. Wise, M.-J. Cheng, D. Sokaras, T.-C. Weng, R. Alonso-Mori, R. C. Davis, J. R. Bargar, J. K. Nørskov, A. Nilsson and A. T. Bell, Journal of the American Chemical Society, 2015, 137, 1305-1313.
71.J. Lin, P. Wang, H. Wang, C. Li, X. Si, J. Qi, J. Cao, Z. Zhong, W. Fei and J. Feng, Advanced Science, 2019, 6.
72.S. Hao, L. Chen, C. Yu, B. Yang, Z. Li, Y. Hou, L. Lei and X. Zhang, ACS Energy Letters, 2019, 4, 952-959.
73.M. Q. Yu, L. X. Jiang and H. G. Yang, Chemical Communications, 2015, 51, 14361-14364.
74.B. Zhang, X. Zheng, O. Voznyy and R. Comin, Science, 2016, 352, 333-337.
75.L. Wu, L. Yu, F. Zhang, B. McElhenny, D. Luo, A. Karim, S. Chen and Z. Ren, Advanced Functional Materials, 2020, 31.
76.H.-S. Hu, Y. Li, Y.-R. Shao, K.-X. Li, G. Deng, C.-B. Wang and Y.-Y. Feng, Journal of Power Sources, 2021, 484.
77.X. Zhou, Y. Mo, F. Yu, L. Liao, X. Yong, F. Zhang, D. Li, Q. Zhou, T. Sheng and H. Zhou, Advanced Functional Materials, 2022, 33.
78.Z. Xu, C.-L. Yeh, J.-L. Chen, J. T. Lin, K.-C. Ho and R. Y.-Y. Lin, ACS Sustainable Chemistry & Engineering, 2022, 10, 11577-11586.
79.Q. Quan, Y. Zhang, F. Wang, X. Bu, W. Wang, Y. Meng, P. Xie, D. Chen, W. Wang, D.

Li, C. Liu, S. Yip and J. C. Ho, Nano Energy, 2022, 101.
80.X. Wang, H. Tian, L. Zhu, S. Li and X. Cui, Nanomaterials, 2024, 14.
81.S. Sidra, V. H. Hoa and D. H. Kim, Journal of Energy Chemistry, 2025, 103, 264-273.
82.M. A. Habib, S. A. Dristy, S. Lin, M. H. Joni, M. Najibullah, R. Mandavkar and J. Lee, Advanced Materials Technologies, 2025, 10.
83.L. Wang, Z. Huang, H. Huang, S. Zhong, M. Huang, T. T. Isimjan and X. Yang, Electrochimica Acta, 2022, 404.
84.Y. Li, K. Xiao, C. Huang, J. Wang, M. Gao, A. Hu, Q. Tang, B. Fan, Y. Xu and X. Chen, Nano-Micro Letters, 2020, 13.
85.D. Li, Z. Li, R. Zou, G. Shi, Y. Huang, W. Yang, W. Yang, C. Liu and X. Peng, Applied Catalysis B: Environment and Energy, 2022, 307.
86.Y. Li, X. Yu, J. Gao and Y. Ma, Chemical Engineering Journal, 2023, 470.
87.P. Wang, Y. Luo, G. Zhang, M. Wu, Z. Chen, S. Sun and Z. Shi, Small, 2021, 18.
88.X. Guo, M. Li, L. He, S. Geng, F. Tian, Y. Song, W. Yang and Y. Yu, Nanoscale, 2021, 13, 14179-14185.
89.L. Chen, Y. Wang, X. Zhao, Y. Wang, Q. Li, Q. Wang, Y. Tang and Y. Lei, Journal of Materials Science & Technology, 2022, 110, 128-135.
90.Q. Che, Q. Li, Y. Tan, X. Chen, X. Xu and Y. Chen, Applied Catalysis B: Environmental, 2019, 246, 337-348.
91.H. Jiang, S. Zhang, Q. Fu, L. Yan, J. Zhang and X. Zhao, Molecules, 2023, 28.
92.M. A. H. S. Lin, R. Mandavkar, R. Kulkarni, S. Burse, Y. U. Chung, C. Liu, Z. Wang, S. Lin, J. H. Jeong, J. Lee, Adv. Sustain. Syst, 2022, 6, 2270022.
93.R. Mandavkar, M. A. Habib, S. Lin, R. Kulkarni, S. Burse, J.-H. Jeong and J. Lee, Applied Materials Today, 2022, 29.
94.H. Zhao and Z.-Y. Yuan, Smart Materials and Devices, 2025, https://doi.org/10.70401/smd.2025.0013.
95.Y. Wang, Q. Ye, L. Lin, Y. Zhao and Y. Cheng, Journal of Colloid and Interface Science, 2023, 651, 1008-1019.
96.Y. Yang, Q. Liu, H. Wang, H. Wen, Z. Peng, K. Xiang, C. Gao, X. Wu, B. Li and Z. Liu, ACS Omega, 2021, 6, 10234-10241.
97.S. Lin, R. Mandavkar, M. A. Habib, S. A. Dristy, M. H. Joni, J.-H. Jeong and J. Lee, Journal of Colloid and Interface Science, 2025, 677, 587-598.
98.M. Zhao, S. Zhang, Y. Hu, H. Xing, C. Li, W. Yuan, W. Sun, C. Guo and C. M. Li, International Journal of Hydrogen Energy, 2024, 51, 998-1009.